Metatranscriptomic and thermodynamic insights into medium-chain fatty acid production using an anaerobic microbiome

Matthew J. Scarborough[1,2], Christopher E. Lawson[2], Joshua J. Hamilton[3,4], Timothy J. Donohue[1,3], and Daniel R. Noguera[1,2]*

Running Title: MCFA Producing Anaerobic Microbiome

[1]The Great Lakes Bioenergy Research Center
University of Wisconsin – Madison
Madison, WI
[2]Department of Civil and Environmental Engineering
University of Wisconsin – Madison
Madison, WI
[3]Department of Bacteriology
University of Wisconsin – Madison
Madison, WI
[4]Department of Biochemistry
University of Wisconsin – Madison
*Corresponding author e-mail: dnoguera@wisc.edu

Abstract

Biomanufacturing from renewable feedstocks represents a sustainable strategy to offset fossil fuel-based chemical production. One potential biomanufacturing strategy is production of medium chain fatty acids (MCFA) from organic feedstocks using either pure cultures or microbiomes. While the set of microbes in a microbiome can often metabolize more diverse organic materials than a single species, and the role of specific species may be known, knowledge of the carbon and energy flow within and between organisms in MCFA producing microbiomes is only starting to emerge. Here, we integrate metagenomic, metatranscriptomic, and thermodynamic analyses to predict and characterize the metabolic network of an anaerobic microbiome producing MCFA from organic matter derived from lignocellulosic ethanol fermentation conversion residue. A total of 37 high quality (>80% complete, < 10% contamination) metagenome-assembled genomes (MAGs) were recovered from the microbiome and metabolic reconstruction of the 10 most abundant MAGs was performed. Metabolic reconstruction combined with metatranscriptomic analysis predicted that organisms affiliated with *Lactobacillus* and Coriobacteriaceae degraded carbohydrates and fermented sugars to lactate and acetate. Lachnospiraceae and Eubacteriaceae affiliated organisms were predicted to transform these fermentation products to MCFA. Thermodynamic analyses identified conditions in which H_2 is expected to be either produced or consumed, suggesting a potential role of H_2 partial pressure on MCFA production. From an integrated systems analysis perspective, we propose that MCFA production could be improved if microbiomes are engineered to use homofermentative instead of heterofermentative *Lactobacillus*, and if MCFA-producing

46 organisms are engineered to preferentially use a thioesterase instead of a CoA transferase
47 as the terminal enzyme in reverse β-oxidation.
48
49
50 **Importance**
51 Mixed communities of microbes play important roles in health, the environment,
52 agriculture, and biotechnology. While tapping the combined activity of organisms within
53 microbiomes may allow the utilization of a wider range of substrate over the use of pure
54 cultures for biomanufacturing, harnessing the metabolism of these mixed cultures remains
55 a major challenge. Here, we predict metabolic functions of bacteria in a microbiome that
56 produces medium-chain fatty acids from a renewable feedstock. Our findings lay the
57 foundation to begin addressing how to engineer and control microbiomes for improved
58 biomanufacturing; to build synthetic mixtures of microbes that produce valuable chemicals
59 from renewable resources; and to better understand microbial communities that
60 contribute to health, agriculture, and the environment.

61 **Introduction**

62 Biological production of chemicals from renewable resources is an important step to
63 reduce societal dependence on fossil fuels. One approach that shows potential for the
64 biological production of chemicals from renewable resources, the carboxylate platform (1,
65 2), uses anaerobic microbial communities to biotransform complex substrates into
66 carboxylic acids, including medium-chain fatty acids (MCFA). MCFA such as hexanoate (a
67 six carbon monocarboxylate, C6) and octanoate (an eight carbon monocarboxylate, C8) are
68 used in large quantities for the production of pharmaceuticals, antimicrobials, and
69 industrial materials, and can be processed to chemicals currently derived from fossil fuels
70 (3, 4).

71 Previous applications of the carboxylate platform have focused on converting
72 organics from undistilled corn beer (5, 6), food (7, 8), winery residue (9), thin stillage from
73 corn ethanol production (10), and lignocellulose-derived materials (11-13) to MCFA, and as
74 we have shown for lignocellulosic biofuel production (4), one can anticipate economic
75 benefits of converting organic residues from these industries into MCFA.

76 MCFA producing bioreactors contain diverse microbial communities (4, 5, 12).
77 While the roles of some community members in these microbiomes can be inferred from
78 studies with pure cultures and from phylogenetic relationships (10, 12, 14, 15), detailed
79 knowledge of specific metabolic activities in many members of these microbiomes is only
80 starting to emerge (16). In general, some community members participate in hydrolysis
81 and fermentation of available organic substrates, while others are involved in the
82 conversion of intermediates to MCFA via reverse β-oxidation, a process also known as
83 chain elongation (1). In reverse β-oxidation, an acyl-CoA unit is combined with acetyl-CoA,

84 with each cycle elongating the resulting carboxylic acid by two carbons(1). Energy
85 conservation in organisms using reverse β-oxidation as the main metabolic process for
86 growth relies on ATP generation with reduced ferredoxin, which is generated through both
87 pyruvate ferredoxin oxidoreductase and an electron bifurcating acyl-CoA dehydrogenase
88 (17). A proton translocating ferredoxin, NAD_ reductase, is used to reduce NAD with
89 ferredoxin and create an ion motive force which is used to generate ATP (17). The even-
90 chain butyric (C4), hexanoic (C6), and octanoic (C8) acids are all potential products of
91 reverse β-oxidation when the process is initiated with acetyl-CoA. The odd-chain valeric
92 (C5) and heptanoic (C7) acids are products of reverse β-oxidation when the chain
93 elongation process starts with propionyl-CoA. While there are demonstrations of this wide
94 range of possible products from chain elongation (5, 18), and MCFA-bioreactors typically
95 produce more than one product (4, 12, 14, 15, 19, 20), a strategy to control the final
96 product length has not yet emerged. We are interested in obtaining the knowledge needed
97 for the rational development and implementation of strategies to improve MCFA yields and
98 control product formation in MCFA-producing microbiomes.
99 Earlier we reported on a bioreactor that produced a mixture of C2, C4, C6 and C8
100 from lignocellulosic stillage (4). Based on 16S rRNA tag sequencing, we found that five
101 major genera, three Firmicutes (*Lactobacillus*, *Roseburia*, *Pseudoramibacter*) and two
102 Actinobacteria (*Atopobium*, *Olsenella)*, represented more than 95% of the community (4).
103 Based on the phylogenetic association of these organisms, the *Lactobacillus* and the
104 Actinobacteria were hypothesized to produce lactic acid, while *Roseburia* and
105 *Pseudoramibacter* were hypothesized to produce the even-chain C4, C6, and C8 acids (4).
106 Furthermore, lactic acid was proposed as the key fermentation product that initiated chain

107 elongation in the microbiome (4). However, since phylogenetic association is not enough to
108 understand in detail the metabolism of these organisms, the earlier study did not generate
109 sufficient knowledge to help understand how to control a MCFA-producing microbiome.
110 Here we report on further studies of the MCFA-producing microbiome reported
111 earlier (4), where we utilized a combination of metagenomic, metatranscriptomic, and
112 thermodynamic analyses to reconstruct the combined metabolic activity of the microbial
113 community. We analyzed the gene expression patterns of the ten most abundant
114 community members during steady-state reactor operation. Our results identify several
115 community members that expressed genes predicted to be involved in complex
116 carbohydrate degradation and in the subsequent fermentation of degradation products to
117 lactate and acetate. Genes encoding enzymes for reverse β-oxidation were expressed by
118 two abundant organisms affiliated with the class Clostridia. Based on a thermodynamic
119 analysis of the proposed MCFA-producing pathways, we predict that individual Clostridial
120 organisms use different substrates for MCFA production (lactate, versus a combination of
121 xylose, H_2, and acetate). We also show that, under certain conditions, production of MCFA
122 provides energetic benefits compared to production of butyrate, thus generating
123 hypotheses for how to control the final products of chain elongation. This knowledge lays a
124 foundation to begin addressing how to engineer and control MCFA producing microbiomes.

125 **Results**

126 **Microbiome characterization**

127 We previously described the establishment of a microbiome that produces MCFA in
128 a bioreactor that is continuously fed with the residues from lignocellulosic ethanol
129 production (4). The reactor feed, identified as conversion residue (CR) in Fig. 1, contained

130 high amounts of xylose, carbohydrate oligomers, and uncharacterized organic matter. To
131 gain insight into the microbial activities that were associated with this MCFA-producing
132 microbiome, samples were collected for metagenomic analysis at five different times (Days
133 12, 48, 84, 96, and 120), and RNA was prepared for metatranscriptomic analysis at Day 96.
134 At the time of metatranscriptomic sampling, the bioreactor converted 16.5% of the organic
135 matter (measured as chemical oxygen demand (COD)) in conversion residue to C6 and C8.
136 During the period of reactor operation described in Fig. 1, the bioreactor converted 16.1 ±
137 3.1 % of COD to C6 and C8, and, therefore, Day 96 is representative of the overall reactor
138 performance.

139 From the metagenomic samples, a total of 219 million DNA reads were assembled
140 and binned, resulting in 37 high quality (>80% complete, <10% contamination) MAGs
141 (Supplement 1). In this study, MAGs are the collection of genes that were assembled into
142 contigs and represent the population of organisms associated with this collection. For the
143 Day 96 sample, 90% of the DNA reads mapped to the ten most abundant MAGs, and each
144 individual MAG mapped to either more than 0.9% of the DNA reads or more than 0.9% of
145 the cDNA reads (Supplement 2).. Abundance of the top 10 MAGs was calculated from the
146 percent of the total DNA reads mapped to the MAGs (Fig. 1c). For the Day 96 sample,
147 relative abundance and expression were compared (Fig. 2; Supplement 2). The most
148 abundant MAGs include a Lachnospiraceae (LCO1, 50%), a *Lactobacillus* (LAC1, 30%), a
149 Coriobacteriacea (COR1, 6.3%), and a Eubacteriaceae (EUB1, 6.0%). Four additional
150 *Lactobacilli* and two additional Coriobacteriacea are also predicted to be within the 10
151 most abundant MAGs (Fig. 2). The other MAGs (Supplement 1) corresponded to Firmicutes

152 (17 MAGs), Actinobacteria (4 MAGs), Tenericutes (3 MAGs), Bacteroidetes (2 MAGs), and
153 Spirochaetes (1 MAG).
154 The metatranscriptome data, obtained from the Day 96 sample, contained 87
155 million cDNA reads. After quality checking and removal of rRNA sequences, 82.6 million
156 predicted transcript reads were used for mapping to MAGs. Of these, 85.3% of the
157 predicted transcripts (hereafter referred to as transcripts or mRNA) mapped back to the 10
158 most abundant MAGs (Supplement 2). Relative expression was calculated from the total
159 filtered mRNA mapped to the MAGs and normalized to the predicted genome length of
160 these bacteria (Fig. 2). MAGs with the highest levels of transcripts included LAC1 (60%),
161 EUB1 (12%), LCO1 (11%), and COR1 (6.3%), which also displayed high abundance in the
162 metagenome (Fig. 2). Whereas LCO1 was most abundant based on DNA reads, LAC1
163 appeared to have the highest activity based on transcript levels.
164 A phylogenetic tree of the ten most abundant MAGs was constructed based on
165 concatenated amino acid sequences of 37 single-copy marker genes (Fig. 3). All Bacilli
166 MAGs (LAC1, LAC2, LAC3, LAC4, and LAC5) clustered with *Lactobacillus.* Average
167 nucleotide identity (ANI) calculations with other *Lactobacillus* genomes were above the 95-
168 96% ANI suggested for species demarcation (21), indicating that these MAGs represent
169 strains of established *Lactobacillus* species (Supplement 3). Clostridia EUB1 clustered with
170 *Pseudoramibacter alactolyticus.* The ANI calculations for this MAG with *P. alactolyticus* and
171 related members of the Eubacteriaceae indicated that EUB1 could represent a new genus
172 within the Eubacterium (Supplement 3). The EUB1 MAG is likely the same organism as
173 represented by the *Pseudoramibacter* operational taxonomic unit (OTU) in the 16S rRNA-
174 based identification reported earlier (4). The Clostridia LCO1 did not cluster with a specific

175 genus; ANIs of the LCO1 MAG and related organisms suggest this MAG could represent a
176 novel genus within the Lachnospiraceae (Supplement 3), while the 16S rRNA-based
177 analysis misclassified it as belonging to the *Roseburia* genus (4). The three Actinobacteria
178 MAGs, COR1, COR2, and COR3, clustered within the Coriobacteriaceae family. One of these
179 MAGs (COR2) clustered with *Olsenella umbonata* (22), but the ANI calculation did not
180 support this MAG being a representative of the *Olsenella* genus (Supplement 3). The other
181 two MAGs (COR1 and COR3) formed their own cluster within the Coriobacteriacea, but
182 were sufficiently different in ANI calculations to suggest that each represents new genera
183 within the Coriobacteriaceae. Phylogenetic classification of the other MAGs obtained in this
184 study are provided in Supplement 1.

185 **Genomic predictions of chemical transformations in the microbiome**

186 A prediction of metabolic networks in the microbiome was performed by analysis of
187 gene annotations or each of the abundant MAGs, whereas expression of the metabolic
188 network was analyzed by mapping mRNA reads to the open reading frames (ORFs) within
189 each of the ten most abundant bacteria. Metabolic reconstruction was performed with
190 automated prediction algorithms (23) and manual curation, particularly of proposed sugar
191 utilization, fermentation and chain elongation pathways (Supplement 4) (1). This analysis
192 identified a set of genes that could be used to model the metabolic potential of the
193 microbiome and also a set of genes with high expression levels in the metatranscriptome.
194 These gene sets were used to analyze the metabolic potential of the microbiome to [1]
195 degrade complex carbohydrates remaining in ethanol conversion residue; [2] transform
196 simple sugars into the fermentation products acetate, lactate, and ethanol; and [3] produce

197 butyrate (C4), C6, and C8 from sugars and fermentation products. The predictions for each
198 of these processes are summarized below.
199 ***Degradation of complex carbohydrates.*** Carbohydrates were a large portion of the
200 organic substrates present in the ethanol conversion residue fed to the bioreactor, and
201 uncharacterized carbohydrates. Quantitative analyses indicated that xylose was the most
202 abundant monosaccharide in the residue, accounting for 22% of the organic matter.
203 Glucose was undetected in most samples or a minor component, and other carbohydrates
204 corresponded to 20% of the organic matter in the residue (see CR bar in Fig. 1).
205 Approximately 40% of the uncharacterized carbohydrates were being degraded at the time
206 the metatranscriptomic samples were obtained (Day 96; Fig. 1).
207 To investigate the expression of genes related to degradation of complex
208 carbohydrates, we analyzed the predicted MAG ORFs using the carbohydrate-active
209 enzyme (CAZyme) database (24). Of particular interest was production of predicted
210 extracellular enzymes that hydrolyze glycosidic bonds in complex carbohydrates, as these
211 may release sugars that can be subsequently metabolized by community members that do
212 not express complex carbohydrate degrading enzymes. The subcellular localization
213 software, CELLO, was used to predict whether individual CAZyme proteins were located
214 within the cytoplasm or targeted to the extracellular space (Supplement 5) (25).
215 This analysis showed that transcripts encoding genes for several types of glycoside
216 hydrolases (GHs) were abundant in several MAGs in the microbiome (Fig. S1). All LAC
217 MAGs expressed genes encoding extracellular CAZymes that cleave glycosidic bonds
218 between hexose and pentose moieties in xylans. In particular, LAC1 LAC2, and LAC4
219 expressed genes that encode several extracellular exo-β-xylosidases that could remove

220 terminal xylose molecules from xylans present in the conversion residue (GH43 and
221 GH120; Fig. S1; Supplement 5). LAC2 also had high levels of transcripts for an exo-α-L-1,5-
222 arabinanase (GH93), predicted to release other pentose sugars from arabinan, which
223 accounts for 3% of the sugar polymers in switchgrass (26, 27). In addition, the COR1, COR3
224 and LAC4 members of the community had high transcript levels for three extracellular
225 CAZymes (GH13) that are predicted to degrade a variety of glucans that may be remaining
226 in switchgrass conversion residue (28). In sum, this analysis predicts that at the time of
227 sampling glucans were degraded by populations represented by *Lactobacillus* and
228 Coriobacteriaceae MAGs, where the populations represented by the LAC MAGs may also
229 have degraded xylans and arabinans. It further suggests that this microbiome is capable of
230 releasing oligosaccharides and sugar monomers from glucans, xylans, and arabinans, the
231 primary components of switchgrass and other plant biomass. The analysis also predicts
232 that LCO1 and EUB1 are not participating in complex carbohydrate degradation.
233 Bacterial oligosaccharide hydrolysis can also occur in the cytoplasm. All MAGs in
234 this microbiome contained predicted cytoplasmic GH13 enzymes, which are known to
235 degrade hexose oligosaccharides. The microbiome also contained abundant transcripts for
236 genes encoding predicted cytoplasmic CAZYmes that degrade maltose (GH4, GH65), a
237 glucose dimer that may result from extracellular breakdown of glucans (Fig. S1).
238 Transcripts encoding known or predicted cytoplasmic β-glucosidases (GH1, GH3) and β-
239 galactosidases (GH2) are found across the MAGs (Fig. S1). In addition, transcripts that
240 encode β-xylosidases (GH1, GH3) and α-L-arabinofuranosidases (GH2), are found in all the
241 LAC MAGs except LAC3 (Fig. S1). Based on the metatranscriptomic analysis, other
242 cytoplasmic CAZymes predicted to hydrolyze pentose-containing oligosaccharides are

243 predicted to be expressed by the LAC1, LAC2, LAC4, and LAC5 members of this microbiome
244 (Fig. S1).
245 ***Transport and production of simple fermentation products from sugars.*** Simple sugars
246 are abundant in ethanol conversion residue and produced during complex carbohydrate
247 hydrolysis. Sugars are therefore expected to be a major substrate for the microbiome.
248 Despite the use of a yeast strain that was engineered for improved xylose utilization in the
249 ethanol fermentation, xylose was the major abundant monosaccharide present in the
250 remaining conversion residue (CR; Fig. 1). As discussed above, the relative transcript levels
251 of genes encoding extracellular GHs (Fig. S1) by several MAGs in the microbiome predict
252 that additional pentoses and hexoses may be released through degradation of complex
253 carbohydrates.
254 We therefore analyzed the genomic potential of the community to transport sugars, and
255 metabolize them to fermentation products, particularly the known MCFA precursors
256 lactate, acetate, and ethanol. To investigate the ability of the community to transport
257 sugars, MAG ORFs were annotated with the Transporter Classification Database
258 (Supplement 6). Expression of genes associated with the pentose phosphate pathway,
259 phosphoketolase pathways, and glycolysis (Fig. 4a) was analyzed to predict the potential
260 for sugar metabolism within individual MAGs.
261 This analysis found that transcripts from genes encoding predicted carbohydrate
262 transporters were among the most highly abundant mRNAs across the microbiome,
263 accounting for 5.8% of the total transcripts . These putative transporters belonged to a
264 variety of families, including many associated with the ATP-binding cassette (ABC)
265 superfamily, and the phosphotransferase system (PTS) family (TD 4.A.-) (Fig. S2). LCO1,

266 LAC1, LAC2, and LAC3 are predicted to contain xylose transporters (XylT) (Fig. 4a), while
267 glucose (GluT), fructose (FruT), and other hexose transporters were expressed across the
268 LAC, COR, and LCO MAGs (Fig. 4a; Fig. S2). EUB1 only encoded transcripts encoding
269 carbohydrate transporters for uptake of fructose and sucrose (Fig. S2). Overall, this
270 analysis predicts that all MAGs have the potential to transport hexose sugars into the cell,
271 while gene expression patterns observed for the LCO1 and the *Lactobacillus* MAGs
272 (excluding LAC3) predicted that at the time of sampling they played a major role in
273 pentose utilization in this microbiome.

274 We also analyzed the metatranscriptomic data to investigate potential routes for sugar
275 metabolism. Once transported to the cytoplasm, glucose can be phosphorylated with
276 hexokinase (HK) and converted to fructose-6-phosphate (F-6-P) by glucose-6-phosphate
277 isomerase (GI). Transcripts encoding predicted HK and GI enzymes are abundant for all
278 MAGs within the microbiome (Fig. 4a), except LAC5 for which the assembly does not show
279 homologues of these proteins. Fructose utilization starts with phosphorylation during
280 transport (Fig. 4a). Fructose-6-phosphate (F-6-P) is either phosphorylated to fructose-1,6-
281 bisphosphate (F-1,6-BP) by phosphofructokinase (PFK) in glycolysis or is cleaved to acetyl-
282 P (Ac-P) and erythrose-4-P (E-4-P) by phosphoketolase (PK). While LAC1, LAC2, LAC4,
283 LAC5 and COR3 all lack homologues of genes encoding PFK (a highly-conserved glycolysis
284 enzyme known to be a major target for regulatory control in hexose utilization) (29), they
285 all contain transcripts for homologues of PK (Fig. 4a). In sum, these analyses predict that all
286 of the abundant MAGs in this microbiome can utilize hexoses that may be produced during
287 hydrolysis of complex oligosaccharides.

288 Transcripts predicted to encode enzymes to convert xylose to xylulose-5-phosphate,
289 xylose isomerase (XI) and xylulose kinase (XK) (30), were abundant in most of the
290 *Lactobacillus* MAGs and LCO1, and either absent or showed very low abundance in LAC3,
291 EUB1 and the COR MAGs (Fig. 4a). Once produced, xylulose-5-P can be degraded through
292 either the phosphoketolase pathway or the pentose phosphate pathway. Transcripts from a
293 gene predicted to encode the diagnostic enzyme of the phosphoketolase pathway,
294 phosphoketolase (PK), which splits xylulose-5-P (X-5-P) into acetyl-P (Ac-P) and
295 glyceraldehyde-3-P (G-3-P), were among the most abundant mRNAs in the *Lactobacillus*
296 MAGs and is also present at high levels in LCO1, accounting for 1.5% of the total transcripts
297 (Fig. 4a; Supplement 4). LCO1 and LAC1 also contained transcripts from homologues of all
298 of the genes needed for the pentose phosphate pathway (R5PE, R5PI, TA, TK in Fig. 4a).
299 Overall, this analysis predicted that multiple routes of pentose utilization could be utilized
300 by the MAGs in this microbiome.
301 The predicted routes for both hexose and xylose metabolism in this microbiome lead to
302 pyruvate production (Fig. 4a), so we also analyzed how this and other fermentation
303 products might lead to MCFA production in this community. All MAGs contained transcripts
304 encoding lactate dehydrogenase homologues (LDH) (Fig. 4a), an enzyme which reduces
305 pyruvate to lactate. Transcript analysis also predicts that all of the MAGs (except LAC3) can
306 oxidize pyruvate to acetyl-CoA, utilizing either pyruvate dehydrogenase (PDH) or pyruvate
307 flavodoxin oxidoreductase (PFOR) (Fig. 4a). All MAGs (except EUB1) contain transcripts
308 encoding homologues of acetate kinase (ACK), which converts acetyl-phosphate (Ac-P) to
309 acetate while producing ATP (Fig. 4a). Based on predictions of the gene expression data,
310 the COR and LAC MAGs are also able to convert acetyl-CoA (Ac-CoA) to ethanol with

311 aldehyde dehydrogenase (ADA) and alcohol dehydrogenase (ADH). In summary, analysis of
312 the gene expression patterns in the conversion residue microbiome predicts that the MAGs
313 in the LCO, LAC and COR ferment sugars to acetate and lactate, while the LAC and COR
314 members produce ethanol as an additional fermentation product.

315 ***Elongation of fermentation products to MCFAs.*** Based on the above findings, we analyzed
316 the microbiome gene expression data to predict which members of the microbiome had the
317 potential for conversion of predicted fermentation products to MCFA. The Clostridia (LCO1
318 and EUB1) are the only MAGs that contained genes encoding homologues of genes known
319 to catalyze chain elongation reactions in the reverse β-oxidation pathway (Fig. 4b). Thus,
320 the subsequent analysis is based on the prediction that only LCO1 and EUB1 are the major
321 producers of MCFA in this microbiome. Furthermore, based on the analysis of sugar
322 utilization above, we predict that LCO1 is the only microorganism in the community that
323 can directly utilize sugars for MCFA production.

324 Acetate, lactate and ethanol, are all fermentation products that would require
325 transformation to acetyl-CoA before being used as a substrate for elongation by the reverse
326 β-oxidation pathway. Acetate could be converted to acetyl-CoA utilizing ATP via acetyl-CoA
327 synthase (ACS) or the ACK and phosphate acetyltransferase (PTA) route (Fig. 4b).
328 Alternatively, acetate can be converted to acetyl-CoA with a CoA transferase (CoAT) which
329 transfers a CoA from one carboxylic acid to another (e.g., from butyryl-CoA to acetate,
330 producing butyrate and acetyl-CoA) (Fig. 4b). Genes encoding homologues of ACS and ACK
331 were not found in EUB1, but LCO1 contained abundant transcripts that encoded
332 homologues of both ACK and PTA (Fig. 4a). Both MAGs also contained transcripts predicted

333 to encode CoAT enzymes (Fig. 4b). Taken together, this analysis predicts that acetate may
334 be used as a substrate for MCFA production by LCO1 and EUB1.
335 Lactate has been proposed as a key intermediate in other microbiomes producing
336 MCFA (12). While transcripts encoding genes for lactate production were abundant in the
337 microbiome (Fig. 4a), lactate did not accumulate to detectable levels during steady
338 operation, but transiently accumulated when the bioreactor received a higher load of
339 conversion residue (4). Transcripts for a gene encoding a predicted lactate transporter
340 (LacT) were abundant in EUB1. In addition, the assembly of LCO1 did not reveal the
341 presence of lactate transporter genes in this MAG, suggesting that only EUB1 may utilize
342 the lactate produced by other MAGs. Neither EUB1 nor LCO1 accumulated transcripts
343 encoding a predicted ADA homologue, which would be required for conversion of
344 acetaldehyde to acetyl-CoA during utilization of ethanol (Fig. 4b). This indicates that if
345 ethanol is produced in this microbiome, it is not used as a significant substrate for MCFA
346 production. Moreover, since ethanol did not accumulate in the reactor during either steady
347 state operation (Fig. 1) or after a high load of conversion residue (4), we predict that
348 ethanol is not a substrate for MCFA production in this microbiome. Rather, based on the
349 predicted activity of LAC and COR MAGs producing lactate and that of EUB1 consuming
350 lactate, we predict that lactate is a key fermentation intermediate for MCFA production.
351 Within the reverse β-oxidation pathway (Fig. 4b), a key enzyme is an electron-
352 bifurcating acyl-CoA dehydrogenase (ACD) containing two electron transfer flavoproteins
353 (EtfA, EtfB) that pass electrons from NADH to ferredoxin (Fig. 4b) (31). This electron
354 bifurcating complex has been recognized as a key energy conserving mechanism in strictly
355 anaerobic bacteria and archaea (17, 31) and studied in detail in butyrate producing

356 anaerobes (32, 33). Transcripts for genes encoding a homologue of the acyl-CoA
357 dehydrogenase complex (ACD, EtfA, EtfB) were abundant in both LCO1 and EUB1, as are
358 those from other genes predicted to be involved in this pathway (Fig. 4b). Chain elongation
359 by the reverse β-oxidation pathway conserves energy by increasing the ratio of reduced
360 ferredoxin (a highly electropositive electron carrier) to the less electropositive NADH (1).
361 In organisms that use this pathway, oxidation of ferredoxin by the Rnf complex generates
362 an ion motive force, and ATP synthase utilizes the ion motive force to produce ATP (17).
363 We found that transcripts for genes encoding homologues of all six subunits of the Rnf
364 complex were abundant in both EUB1 and LCO1 (RnfABCDEG, Fig. 4b). To maintain
365 cytoplasmic redox balance, reduced ferredoxin could transfer electrons to H^+ via
366 hydrogenase, generating H_2. LCO1 and EUB1, along with the COR MAGs, contained
367 abundant transcripts for genes predicted to produce ferredoxin hydrogenase (H2ase, Fig.
368 4b), supporting the hypothesis that H_2 production plays a role within this MCFA-producing
369 microbiome. We also looked for two additional hydrogenases known to conserve energy
370 either through the translocation of protons (EchABCDEF Fig. 4b,) or by electron
371 confurcation, utilizing electrons from both NADH and reduced ferredoxin (HydABC, Fig. 4b)
372 (17). It does not appear that these systems play a major role in H_2 production in this
373 microbiome since none of the MAGs contained genes encoding homologues of the known
374 components for either of these enzyme complexes (Fig 5b).

375 **Thermodynamic analysis of MCFA production in the microbiome**

376 The above analysis predicted several potential routes for MCFA production by LCO1
377 and EUB1 in this microbiome. To evaluate the implications of these potential chain
378 elongation routes, we used thermodynamic analysis to investigate the energetics of the

379 predicted transformations. For this, we reconstructed metabolic pathways for xylose and
380 lactate conversion, as well as ATP yields based on the data obtained from gene expression
381 analyses (Tables S2-S3, Supplement 7). Metabolic reconstructions considered xylose (Table
382 S2) and lactate (Table S3) as major substrates for synthesis of C4, C6, and C8 products. In
383 addition, both LCO1 and EUB1 have the potential to use a CoAT or a thioesterase (TE) as
384 the terminal enzyme of the reverse β-oxidation pathway (Fig. 4b), so we considered both
385 possibilities in the thermodynamic analysis. We used these reconstructions to calculate the
386 free energy changes of the overall biochemical reactions assuming an intracellular pH of
387 7.0, a temperature of 35°C, and H_2 partial pressures of 1.0×10^{-6}, 1.0, and 6.8 atm for low,
388 standard, and high H_2 partial pressure, respectively. The low value is the approximate
389 concentration of H_2 in water that is in equilibrium with the atmosphere and the high value
390 is an expected maximum in a pressurized mixed culture fermentation system (34). We also
391 compared the efficiency of ATP production to an expected maximum yield of 1 ATP per -60
392 kJ energy generated by the overall chemical transformation (35).
393 The use of xylose as the substrate (Table S2, Eqs. 3-8) is possible for LCO1 but not
394 EUB1, since the later MAG lacks genes to transport and activate xylose to xylulose-5-P
395 (XylT, XI, XK, Fig. 4a). Our analysis predicts that, with a pathway containing a terminal
396 CoAT enzyme, the ATP yield (mol ATP mol^{-1} xylose) does not increase if longer chain
397 MCFAs are produced. However, if TE is used for the terminal step of reverse β-oxidation
398 (Eqs. 6-8), the overall ATP yield is lower, but it increases with increasing product length,
399 and C8 production provides a 17% increase in ATP yield versus production of C4. This
400 suggests that LCO1 has no energetic benefit for producing C6 or C8 solely from xylose
401 unless TE is used as the terminal enzyme of reverse β-oxidation. Additionally, the higher

402 ATP yield of xylose conversion to C4 (Eqs. 3 and 6), in comparison to xylose conversion to
403 lactate and acetate by other members of the microbiome (Eq. 2), may explain why LCO1
404 reached higher abundance in the microbiome compared to the other less abundant MAGs
405 (LAC) that are predicted to ferment xylose to lactate and acetate (Fig. 2). In production of
406 C4 and C8, no H_2 is predicted to be formed if a CoAT is utilized (Eqs. 3 and 5), whereas H_2
407 production is predicted when C6 is produced (Eq. 4). On the other hand, if a TE terminal
408 enzyme is utilized for the reverse β-oxidation, H_2 is predicted to be produced for all
409 carboxylic acid products.

410 Additional metabolic reconstructions analyzed the co-utilization of xylose with a
411 monocarboxylic acid (Table S2, Eq 9-18). This analysis predicted that co-metabolism of
412 these substrates could provide an energetic advantage (i.e., higher mol ATP per mol of
413 xylose) if H_2 is utilized as an electron donor. This suggests that H_2, produced by either
414 EUB1 or COR MAGs (H2ase, Fig5a), may be utilized by LCO1 to support MCFA production. If
415 TE is used as the terminal enzyme of reverse β-oxidation (Eqs. 14-18), there is no increase
416 in ATP yield versus utilization of xylose as the sole carbon source (Eqs. 6-8).

417 We also modeled MCFA production from lactate by EUB1, since the gene expression
418 data suggested that EUB1 could transform lactate to MCFA. In models utilizing CoAT (Table
419 S3, Eq. 19-21) as a final step in MCFA production, the ATP yield increases as longer chain
420 MCFA are produced, but the free energy released is near the expected limit for ATP
421 production (35) under conditions of low H_2 partial pressure and below this limit at high H_2
422 partial pressures (Table S3). If TE is utilized as a final step in MCFA production by EUB1
423 (Eq. 22-24), lower ATP yields are predicted, and in that case the production of longer chain
424 MCFAs has a more pronounced effect on the ATP generated per mol of lactate consumed.

425 For instance, production of C6 results in a 100% increase in the ATP yield compared to
426 producing C4. However, each elongation step reduces the amount of energy released per
427 mol ATP produced, such that production of C8 from lactate results in the release of -58 kJ
428 per ATP produced under high H_2 conditions, which is near the expected limits for a cell to
429 conserve chemical energy as ATP. Overall, the thermodynamic analysis does not
430 unequivocally predict which terminal enzyme may be energetically more advantageous for
431 MCFA production from lactate. While using TE would result in more favorable free energy
432 release than when using CoAT, the predicted ATP yields are lower with TE than with CoAT.
433 We also note that although CoAT transcript abundance was higher than TE transcript
434 abundance (Fig. 4b), expression alone cannot be used as a predictor of which terminal
435 enzyme was primarily used since a kinetic characterization of these enzymes is not
436 available. Regardless, the thermodynamic modeling predicts that, in all conditions, H_2 will
437 be produced during lactate elongation (Table S3), and that TE could be a better terminal
438 enzyme to force production of longer chain acids in order to maximize ATP yield (Table
439 S3).

440 When modeling scenarios utilizing lactate plus carboxylic acids as growth substrates
441 (Table S3, Eqs. 25-36), their elongation by EUB1 would increase the amount of ATP it could
442 produce compared to using lactate only if using a terminal CoAT (Eqs. 19-21). H_2
443 production or consumption is not predicted in these scenarios, and the calculated free
444 energy released per mol of ATP produced (-50 to -53 kJ mol^{-1} ATP) is low, near the
445 physiological limit of -60 kJ mol^{-1} ATP for energy conservation by the cell. Models with TE
446 as the terminal enzyme in reverse β-oxidation were also analyzed (Eqs. 31-36) even though
447 EUB1 is not predicted to have this ability as it lacks ACS and ACK needed to utilize acetate

448 (Fig. 4b). In such models, producing C6 and C8 from lactate plus acetate (Eqs. 32-33) is
449 energetically favorable, whereas C4 production is not (Eq. 31).

450 **Discussion**

451 In this study, we illustrate how combining genomic, computational and thermodynamic
452 predictions can illustrate how a microbial community can convert organic substrates in
453 lignocellulosic conversion residues into MCFA (Fig. 5). Specifically, this approach predicts
454 that the coordinated and step-wise metabolic activity of different members of this
455 microbiome allow cleavage of complex five- and six-carbon containing polysaccharides;
456 conversion of sugars into simple fermentation products; and utilization of sugars and
457 intermediate fermentation products for MFCA production. This approach further predicts
458 the role of intracellular and extracellular reductants in these processes. Below, we illustrate
459 the new insight that has been gained on the activity of a MCFA producing microbiome and
460 how this might relate to other systems.

461 The microbial community studied here is similar in phylogenetic composition to
462 other microbial communities producing MCFA. For instance, in a community fed with dilute
463 ethanol and stillage, *Lactobacillus* and a member of the Clostridium Group IV were
464 abundant (12). In a system producing MCFA using thin stillage produced from corn ethanol,
465 *Lactobacillus* were enriched alongside *Megasphaera*, a known MCFA-producing Firmicute
466 (10). In a reactor converting wastes from wine production to MCFA, *Lactobacillus* and
467 Clostridia related to *Ruminococcus* were enriched (9). In each case, a community containing
468 carbohydrate fermenting organisms and potential MCFA producing organisms emerged.

469 Our data suggest that the contribution of *Lactobacillus* in this microbiome is in
470 extracellular carbohydrate degradation and subsequent metabolism of pentose- and

471 hexose-containing carbohydrates, while Coriobacteriaceae are predicted to metabolize
472 hexose-containing carbohydrates. The combined metabolic activities of these two MAGs
473 would produce oligosaccharides and monomeric sugars that would become available to
474 these and other members of the microbiome. Metabolic reconstruction combined with
475 microbiome transcript levels also suggest that the *Lactobacillus* and Coriobacteriaceae
476 MAGs produce fermentation end products, primarily lactate and acetate, from these
477 carbohydrates. Coriobacteriaceae, however, are also predicted to produce H_2. In addition,
478 microbiome gene expression patterns indicate that two MAGs, EUB1 and LCO1, produce
479 MCFA via reverse β-oxidation. LCO1 is predicted to consume xylose based on gene
480 expression analysis, whereas RNA abundance measurements indicate that EUB1 consumes
481 lactate.

482 We used thermodynamics to analyze hypothetical scenarios of MCFA production by
483 EUB1 and LCO1. Although the comparison of these hypothetical scenarios did not provide
484 an unequivocal answer to how chain elongation occurs in LCO1 and EUB1, it is helpful to
485 generate hypotheses that could eventually be tested in future research. Our
486 thermodynamic analysis predicts that the most energetically advantageous metabolism for
487 LCO1 (based on ATP production per mol xylose consumed) is the consumption of xylose, H_2
488 and carboxylates to produce C4, C6, and C8 while utilizing CoAT as a terminal enzyme.
489 While xylose is a major component of conversion residue (CR, Fig. 1), H_2 is expected to be
490 produced by Coriobacteriaceae MAGs and EUB1. For EUB1, which is expected to utilize
491 lactate, our analysis predicts that production of MCFA produces higher amounts of ATP,
492 with C6 resulting in a 2-fold increase in ATP production versus producing C4 when
493 consuming lactate as a sole substrate.

494 Predictions from our thermodynamic modeling indicate that C8 production from
495 lactate is energetically advantageous. However, this is at odds with C6 being produced from
496 conversion residue at higher concentrations than C8 (Fig. 1). It is known that C8 is a
497 biocide, so it may be that C8 accumulation is limited by the level of tolerance community
498 members have for this product (12). It is also possible that higher C6 production indicates
499 a more important role of C6 production by LCO1 without lactate being an intermediate
500 metabolite. It has also been shown that removal of C8 allows for higher productivities of
501 carboxylate platform systems (1).
502 H_2 production and interspecies H_2 transfer are known to have significant impacts on
503 the metabolism of microbial communities (36). Our analysis predicts a role of H_2 in
504 supporting chain elongation in a carboxylate platform microbiome. While high H_2 partial
505 pressures are proposed to inhibit production of acetate and other carboxylic acids (37, 38),
506 organisms that use the phosphoketolase pathway (the *Lactobacillus* and LCO1 MAGs
507 identified in this study) can produce C2, C4 and C8 without producing H_2 (Table S2, Eqs. 2,
508 3 and 5). While conversion of lactate to MCFA (Table S3, Eqs. 19-24) is predicted to
509 produce H_2, other processes such as co-utilization of xylose and a monocarboxylic acid for
510 MCFA production (Table S2, Eq. 9-18) would consume H_2. Therefore, H_2 accumulation is
511 not expected to limit production of MCFA, although H_2 partial pressures may influence the
512 metabolic routes utilized by the microbiome.
513 In considering how to further improve the production of MCFA with a microbiome,
514 additional work is needed to characterize and engineer reverse β-oxidation proteins from
515 the Firmicutes in order to improve production of organic acids longer than C4. Further, our
516 data predict that the terminal enzyme of reverse β-oxidation can influence production of

517 MCFA. While a CoAT enzyme results in higher ATP production, a TE makes production of
518 MCFA more energetically advantageous by increasing the ATP yield for production of C6
519 and C8 compared to C4 (Tables S2-S3). Therefore, engineering chain-elongating organisms
520 to only have a TE rather than CoAT may improve production of MCFA.

521 Our metabolic reconstructions predict that lactate was a key fermentation product
522 that supports MCFA production. Therefore, strategies to enhance lactate production and
523 minimize other fermentation products (fermentation of carbohydrates to lactate, rather
524 than acetate in this example), could improve production of desired end products.
525 Moreover, designing strategies to enrich a community that produces a critical intermediate
526 like lactate by one pathway (e.g., homofermentative lactate-producing *Lactobacilli*, rather
527 than hetero-fermenters producing both lactate and C2) could improve performance of the
528 microbiome. However, the principles controlling the presence or dominance of
529 heterofermentative versus homofermentative organisms in microbial communities remain
530 largely unexplored. Alternatively, higher production of a desired product, C8, could be
531 achieved by adjusting the abundance or establishing a defined co-culture containing a lactic
532 acid bacterium capable of complex carbohydrate degradation, such as LAC1, and a lactate-
533 elongating organism, such as EUB1. The ability to establish defined synthetic communities,
534 to adjust the abundance of microbiome members or to regulate the metabolic routes within
535 the microbiome may allow more control over the function of a microbiome for production
536 of MCFA or to optimize other traits.

537 In summary, this work demonstrates that one can dissect and model the
538 composition of microbiomes as a way to understand the contribution of different
539 community members to its function. In the case of an anaerobic carboxylate platform

540 microbiome fed lignocellulosic ethanol conversion residue, two Clostridia-related
541 organisms (EUB1 and LCO1) are predicted to be responsible for production of MCFA via
542 reverse β-oxidation. This provides a genome-centric rationale for the previously
543 established correlation between Clostridia-related abundance and MCFA production noted
544 in carboxylate platform systems (4, 12). This study further predicts that the terminal
545 enzyme in product synthesis and the fermentation end products produced by other
546 community members can play a role in determining predominant products of this
547 microbiome. These approaches, concepts and insights should be useful in predicting and
548 controlling MCFA production by reactor microbiomes and in analyzing the metabolic,
549 genomic and thermodynamic factors influencing the function of other microbiomes of
550 health, environmental, agronomic or biotechnological importance.

551 **Methods**

552 **Production of conversion residue.** Switchgrass used to generate conversion residue was
553 treated by ammonia fiber expansion and enzymatically treated with Cellic CTec3® and
554 Cellic HTec3® (Novozymes) to digest cellulose and hemicellulose (to glucose and xylose,
555 primarily) (39). Hydrolysate was fermented with *Saccharomyces cerevisiae* Y128, a strain
556 with improved xylose utilization (40). Fermentation media was distilled to remove ethanol
557 (4).

558 **Bioreactor operation.** The bioreactor was seeded with acid digester sludge from the Nine
559 Springs Wastewater treatment plant in Madison, WI. The retention time of the semi-
560 continuous reactor was maintained at six days by pumping conversion residue into the
561 reactor, pumping reactor effluent from the reactor once per hour, and maintaining a liquid
562 volume of 150mL in the reactor. The reactor was mixed with a magnetic stir bar. The

563 temperature of the reactor was controlled at 35 °C using a water bath, and the pH of the
564 reactor was maintained at 5.5 by feeding 5M KOH through a pump connected to a pH
565 controller. This reactor sustained MCFA production for 252 days (4).
566 **Metabolite analysis.** Samples from the bioreactor and conversion residue were collected
567 for metabolite analysis. All samples were filtered using 0.22 μm syringe filters
568 (ThermoFisher Scientific SLGP033RS, Waltham, MA, USA). Chemical oxygen demand (COD)
569 analysis was performed using High Range COD Digestion Vials (Hach 2125915, Loveland,
570 CO, USA) per standard methods (41). Soluble carbohydrates were measured with the
571 anthrone method (42). Glucose, xylose, acetic acid, formic acid, lactic acid, succinic acid,
572 pyruvic acid, glycerol and xylitol were analyzed with high performance liquid
573 chromatography and quantified with an Agilent 1260 Infinity refractive index detector
574 (Agilent Technologies, Inc. Palo Alto, CA) using a 300 x 7.8 mm Bio-Rad Aminex HPX-87H
575 column with Cation-H guard (BioRad, Inc., Hercules, CA). Acetamide, ethanol, n-propionic
576 acid, n-butyric acid, iso-butyric acid, n-pentanoic acid, iso-pentanoic acid, n-hexanoic acid,
577 iso-hexanoic acid, n-heptanoic acid, and n-octanoic acid were analyzed with tandem gas
578 chromatography-mass spectrometry. An Agilent 7890A GC system (Agilent Technologies,
579 Inc. Palo Alto, CA) with a 0.25 mm Restek Stabilwax DA 30 column (Restek 11008,
580 Belefonte, PA) was used. The GC-MS system was equipped with a Gerstel MPS2 (Gerstel,
581 Inc. Baltimore, MD) auto sampler and a solid-phase micro-extraction gray hub fiber
582 assembly (Supelco, Bellefonte, PA). The MS detector was a Pegasus 4D TOF-MS (Leco Corp.,
583 Saint Joseph, MI). Stable isotope labeled internal standards were used for each of the
584 analytes measured with GC-MS.

585 **DNA and RNA sequencing.** Biomass samples, consisting of centrifuged and decanted 2 mL
586 aliquots, were collected at Day 12, Day 48, Day 84, Day 96, and Day 120 of reactor
587 operations from initial start-up. Samples were also taken at 96 days and flash-frozen in
588 liquid nitrogen for RNA extraction. For DNA extraction, cells were lysed by incubating in a
589 lysis solution (1.5M sodium chloride, 100mM trisaminomethane, 100mM ethylenediamine
590 (EDTA), 75mM sodium phosphate, 1% cetyltrimethylammonium bromide, and 2% sodium
591 dodecyl sulfate(SDS)), lysozyme (Thermo Fisher Scientific, MA, USA), and proteinase K
592 (New England Biolabs,MA, USA). We then added 500 uL of a 24:24:1 solution of phenol:
593 chloroform: isoamyl alcohol and bead-beat samples for 2 minutes. After bead-beating,
594 biomass was centrifuged at 5,000 rcf for 3 minutes and the entire supernatant was
595 transferred to a 1.5 mL centrifuge tube. Samples were centrifuged again at 12,000 rcf for 10
596 minutes and the aqueous layer was then removed to a new centrifuge tube. A second phase
597 separation was then performed using chloroform. After centrifuging again and separating
598 the aqueous phase, 500 uL of isopropanol was added to each samples and samples were
599 then incubated at -20 deg C for 24 hours. Following this incubation, samples were
600 centrifuged at 12,000 rcf for 30 minutes at 4 deg C, decanted, and washed with 70%
601 ethanol. After air-drying the samples, pellets were resuspended in 100 uL of TE buffer and
602 2 uL of 10 mg/mL RNAse was added to each sample. Samples were incubated for 15
603 minutes at 37 deg C. We then added 100uL of a 24:24:1 solution of phenol: chloroform:
604 isoamyl alcohol to each sample and centrifuged at 12,000 rcf for 10 minutes. We
605 separated the aqueous phase to a new centrifuge tube and added 100 Ul of chloroform.
606 Again, samples were centrifuged at 12,000 rcf for 10 minutes and the aqueous phase was
607 separated to a new centrifuge tube. We then added 10 uL of 3M sodium acetate and 250 uL

608 of 95% ethanol to each sample and incubated for 24 hours at -20 deg C. Samples were
609 centrifuged at 12,000 rcf for 30 minutes at 4 deg C and the pellets were washed with 70%
610 ethanol. After air-drying, pellets were resuspended in 50uL of TE buffer. After re-
611 suspending the DNA, quantity, purity, and quality were assessed with a Qubit 4
612 Fluorometer (Thermo Fisher Scientific, MA, USA), a Nanodrop 2000 spectrophotometer
613 (Thermo Fisher Scientific, MA, USA), and gel electrophoresis.

614 For RNA extraction, cells were lysed by incubating in a lysis solution (20 mM sodium
615 acetate, 1 mM EDTA, and 0.5% SDS prepared in diethylpyrocarbonate-treated water
616 (Invitrogen, CA, USA)) and TRIzol (Invitrogen, CA, USA). The treated cells were subjected to
617 2 minutes of bead beating using Lysing Matrix A (MP Biomedicals, CA, USA). After this step,
618 successive phase separations with phenol: chloroform: isoamyl alcohol and chloroform
619 were used to separate nucleic acids from additional cell material, as described above. RNA
620 was further purified with an RNEasy Mini Kit (Qiagen, Hilden, Germany) and on-column
621 DNAse 1 (Qiagen, Hilden, Germany) treatment. After re-suspending the RNA, quantity,
622 purity, and quality were assessed with a Qubit 4 Fluorometer (Thermo Fisher Scientific,
623 MA, USA), a Nanodrop 2000 spectrophotometer (Thermo Fisher Scientific, MA, USA), and
624 gel electrophoresis. RNA samples were submitted to the University of Wisconsin Gene
625 Expression Center for quality control with a Bioanalyzer (Agilent, CA, USA), ribosomal RNA
626 reduction with a RiboZero-Bacteria rRNA Removal Kit (Illumina, CA, USA) with a 1μg RNA
627 input. Strand-specific cDNA libraries were prepared with a TruSeq RNA Library Prep Kit
628 (Illumina, CA, USA).

629 DNA and RNA were sequenced with the Illumina HiSeq 2500 platform (Illumina, CA,
630 USA). For DNA, an average insert size of 550 bp was used and 2 x 250 bp reads were

631 generated. For RNA, 1 x 100 bp reads were generated. Raw DNA and cDNA reads can be
632 found on the National Center for Biotechnology Information (NCBI) website under
633 BioProject PRJNA418244.
634 **Metagenomic assembly, binning, and quality control.** DNA sequencing reads were
635 filtered with Sickle using a minimum quality score of 20 and a minimum sequence length of
636 100 (43). Reads from all five samples were then co-assembled using metaspades and kmer
637 values of 21, 33, 55, 77, 99, and 127 (44). Binning of assembled contigs was performed with
638 MaxBin v2.2.1 (45). The quality, completeness, and contamination of each bin was analyzed
639 with CheckM v1.0.3 (46). Read mapping was performed with BBMAP v35.92
640 (https://sourceforge.net/projects/bbmap) to estimate the relative abundance of each bin.
641 Relative abundance was calculated by normalizing the number of mapped reads to the
642 genome size.
643 **Phylogenetic analysis.** Phylogeny of the draft genomes was assessed using 37 universal
644 single-copy marker genes with Phylosift v1.0.1 (47). In addition to the draft genomes, 62
645 publically-available genomes of related organisms were used to construct a phylogenetic
646 tree. Concatenated amino acid sequences of the marker genes were aligned with Phylosift,
647 and a maximum likelihood phylogenetic tree was constructed with RAxML v8.2.4 with the
648 PROTGAMMAAUTO model and 100 bootstraps (48). ANI calculations were performed
649 using JSpecies (49).
650 **Genome annotations.** Draft genomes were annotated with MetaPathways v2.5.(23) Open
651 reading frames (ORFs) were predicted using Prodigal v2.0 (50), and the ORFs were
652 annotated with the following databases: SEED (accessed March 2013), Clusters of
653 Orthologous Groups (COG, accessed December 2013), RefSeq (accessed January 2017),

654 Metacyc (accessed October 2011), and KEGG (accessed January 2017). The LAST algorithim
655 was used for assigning functional annotations (51). Functional annotations for each MAG
656 are provided in Supplement 4. Draft genomes were further annotated with the CAZY
657 database (24). CELLO was used to determine the subcellular location of the CAZYs (25).
658 Transporters were identified using the Transporter Classification Database.
659 **Transcript analysis.** Analysis of transcript data was performed as described in Lawson, et
660 al. (52). cDNA reads were quality filtered as described above for DNA. SortMeRNA was used
661 to remove rRNA sequences using multiple databases for RNA sequences (53). The
662 remaining non-rRNA sequences were then mapped back to the draft genomes using BBMap
663 v35.92 (https://sourceforge.net/projects/bbmap) with the minimum sequence identity set
664 to 0.95. Ambiguous reads with multiple top-hit mapping locations were assigned to a
665 random ORF. The number of RNA reads mapping to each ORF was calculated with htseq-
666 count v0.6.1 with the "intersection-strict" parameter (54). Relative gene expression
667 (RPKM) was calculated for each ORF by normalizing the number of mapped RNA reads for
668 each ORF to the ORF length and the total number of RNA reads mapping back to the
669 genome. The relative RPKM (relPKM) was then calculated as the ratio of the RPKM for the
670 ORF to the median RPKM across the draft genome. Finally, the $\log_2$(relRPKM) was
671 calculated to determine the log-fold difference. As such, a positive number corresponds to
672 greater than median expression levels and a negative number to expression below median
673 levels.

674 **Acknowledgements**

675 This work was funded by the DOE Great Lakes Bioenergy Research Center (DOE BER
676 Office of Science DE-FC02-07ER64494 and DE-SC0018409). M.J.S. is supported by the

National Science Foundation Graduate Research Fellowship Program under grant No. DGE-1256259. C.E.L is supported by a Postgraduate Scholarship–Doctoral (PGS-D) award from the National Sciences and Engineering Research Council of Canada (NSERC) and a Wisconsin Distinguished Graduate Fellowship. JJH was supported by the National Institute of Food and Agriculture, U.S. Department of Agriculture, under award number 2016-67012-24709. The authors thank Francisco Moya for assistance with RNA extraction and the University of Wisconsin Biotechnology Center DNA Sequencing Facility and Gene Expression Center for library preparation and Illumina sequencing services.

References

1. **Angenent LT, Richter H, Buckel W, Spirito CM, Steinbusch KJJ, Plugge CM, Strik D, Grootscholten TIM, Buisman CJN, Hamelers HVM.** 2016. Chain Elongation with Reactor Microbiomes: Open-Culture Biotechnology To Produce Biochemicals. Environ Sci Technol **50:**2796-2810.
2. **Holtzapple MT, Granda CB.** 2009. Carboxylate platform: the MixAlco process part 1: comparison of three biomass conversion platforms. Appl Biochem Biotechnol **156:**95-106.
3. **Sarria S, Kruyer NS, Peralta-Yahya P.** 2017. Microbial synthesis of medium-chain chemicals from renewables. Nat Biotechnol **35:**1158-1166.
4. **Scarborough MJ, Lynch G, Dickson M, McGee M, Donohue TJ, Noguera DR.** 2018. Increasing the economic value of lignocellulosic stillage through medium-chain fatty acid production. Biotechnology for Biofuels **11:**200.
5. **Agler MT, Spirito CM, Usack JG, Werner JJ, Angenent LT.** 2012. Chain elongation with reactor microbiomes: upgrading dilute ethanol to medium-chain carboxylates. Energy Environ Sci **5:**8189.
6. **Ge S, Usack JG, Spirito CM, Angenent LT.** 2015. Long-Term n-Caproic Acid Production from Yeast-Fermentation Beer in an Anaerobic Bioreactor with Continuous Product Extraction. Environ Sci Technol **49:**8012-8021.
7. **Grootscholten TIM, Strik DPBTB, Steinbusch KJJ, Buisman CJN, Hamelers HVM.** 2014. Two-stage medium chain fatty acid (MCFA) production from municipal solid waste and ethanol. Applied Energy **116:**223-229.
8. **Grootscholten TIM, dal Borgo FK, Hamelers HVM, Buisman CJN.** 2013. Promoting chain elongation in mixed culture acidification reactors by addition of ethanol. Biomass & Bioenergy **48:**10-16.

711 9. **Kucek LA, Xu JJ, Nguyen M, Angenent LT.** 2016. Waste Conversion into n-
712 Caprylate and n-Caproate: Resource Recovery from Wine Lees Using Anaerobic
713 Reactor Microbiomes and In-line Extraction. Front Microbiol **7**.
714 10. **Andersen SJ, Candry P, Basadre T, Khor WC, Roume H, Hernandez-Sanabria E,**
715 **Coma M, Rabaey K.** 2015. Electrolytic extraction drives volatile fatty acid chain
716 elongation through lactic acid and replaces chemical pH control in thin stillage
717 fermentation. Biotechnol Biofuels **8**.
718 11. **Xiong BY, Richard TL, Kumar M.** 2015. Integrated acidogenic digestion and
719 carboxylic acid separation by nanofiltration membranes for the lignocellulosic
720 carboxylate platform. J Membr Sci **489:**275-283.
721 12. **Andersen SJ, De Groof V, Khor WC, Roume H, Props R, Coma M, Rabaey K.** 2017.
722 A Clostridium Group IV Species Dominates and Suppresses a Mixed Culture
723 Fermentation by Tolerance to Medium Chain Fatty Acids Products. Front Bioeng
724 Biotechnol **5:**8.
725 13. **Kenealy WR, Cao Y, Weimer PJ.** 1995. Production of caproic acid by cocultures of
726 ruminal cellulolytic bacteria and Clostridium kluyveri grown on cellulose and
727 ethanol. Applied Microbiology and Biotechnology **44:**507-513.
728 14. **Kucek LA, Nguyen M, Angenent LT.** 2016. Conversion of L-lactate into n-caproate
729 by a continuously fed reactor microbiome. Water Res **93:**163-171.
730 15. **Zhu X, Tao Y, Liang C, Li X, Wei N, Zhang W, Zhou Y, Yang Y, Bo T.** 2015. The
731 synthesis of n-caproate from lactate: a new efficient process for medium-chain
732 carboxylates production. Sci Rep **5:**14360.
733 16. **Han W, He P, Shao L, Lu F.** 2018. Metabolic Interactions of a Chain Elongation
734 Microbiome. Appl Environ Microbiol doi:10.1128/AEM.01614-18.
735 17. **Buckel W, Thauer RK.** 2013. Energy conservation via electron bifurcating
736 ferredoxin reduction and proton/Na(+) translocating ferredoxin oxidation. Biochim
737 Biophys Acta **1827:**94-113.
738 18. **Spirito CM, Richter H, Rabaey K, Stams AJ, Angenent LT.** 2014. Chain elongation
739 in anaerobic reactor microbiomes to recover resources from waste. Curr Opin
740 Biotechnol **27:**115-122.
741 19. **Zhu X, Zhou Y, Wang Y, Wu T, Li X, Li D, Tao Y.** 2017. Production of high-
742 concentration n-caproic acid from lactate through fermentation using a newly
743 isolated Ruminococcaceae bacterium CPB6. Biotechnol Biofuels **10:**102.
744 20. **Nelson R, Peterson D, Karp E, Beckham G, Salvachúa D.** 2017. Mixed Carboxylic
745 Acid Production by Megasphaera elsdenii from Glucose and Lignocellulosic
746 Hydrolysate. Fermentation **3:**10.
747 21. **Kim M, Oh HS, Park SC, Chun J.** 2014. Towards a taxonomic coherence between
748 average nucleotide identity and 16S rRNA gene sequence similarity for species
749 demarcation of prokaryotes (vol 64, pg 346, 2014). Int J Syst Evol Microbiol
750 **64:**1825-1825.
751 22. **Kraatz M, Wallace RJ, Svensson L.** 2011. Olsenella umbonata sp. nov., a
752 microaerotolerant anaerobic lactic acid bacterium from the sheep rumen and pig
753 jejunum, and emended descriptions of Olsenella, Olsenella uli and Olsenella profusa.
754 Int J Syst Evol Microbiol **61:**795-803.

755 23. **Konwar KM, Hanson NW, Bhatia MP, Kim D, Wu SJ, Hahn AS, Morgan-Lang C,**
756 **Cheung HK, Hallam SJ.** 2015. MetaPathways v2.5: quantitative functional,
757 taxonomic and usability improvements. Bioinformatics **31:**3345-3347.
758 24. **Lombard V, Golaconda Ramulu H, Drula E, Coutinho PM, Henrissat B.** 2014. The
759 carbohydrate-active enzymes database (CAZy) in 2013. Nucleic Acids Res **42:**D490-
760 495.
761 25. **Yu CS, Chen YC, Lu CH, Hwang JK.** 2006. Prediction of protein subcellular
762 localization. Proteins **64:**643-651.
763 26. **Zurawski JV, Khatibi PA, Akinosho HO, Straub CT, Compton SH, Conway JM, Lee**
764 **LL, Ragauskas AJ, Davison BH, Adams MWW, Kelly RM.** 2017. Bioavailability of
765 Carbohydrate Content in Natural and Transgenic Switchgrasses for the Extreme
766 Thermophile Caldicellulosiruptor bescii. Appl Environ Microbiol **83**.
767 27. **Sakamoto T, Thibault JF.** 2001. Exo-arabinanase of Penicillium chrysogenum able
768 to release arabinobiose from alpha-1,5-L-arabinan. Appl Environ Microbiol
769 **67:**3319-3321.
770 28. **Abdullah M, French D.** 1970. Substrate Specificity of Pullulanase. Arch Biochem
771 Biophys **137:**483-&.
772 29. **Ronimus RS, Morgan HW.** 2001. The biochemical properties and phylogenies of
773 phosphofructokinases from extremophiles. Extremophiles **5:**357-373.
774 30. **Lawlis VB, Dennis MS, Chen EY, Smith DH, Henner DJ.** 1984. Cloning and
775 sequencing of the xylose isomerase and xylulose kinase genes of Escherichia coli.
776 Appl Environ Microbiol **47:**15-21.
777 31. **Demmer JK, Pal Chowdhury N, Selmer T, Ermler U, Buckel W.** 2017. The
778 semiquinone swing in the bifurcating electron transferring flavoprotein/butyryl-
779 CoA dehydrogenase complex from Clostridium difficile. Nat Commun **8:**1577.
780 32. **Li F, Hinderberger J, Seedorf H, Zhang J, Buckel W, Thauer RK.** 2008. Coupled
781 ferredoxin and crotonyl coenzyme a (CoA) reduction with NADH catalyzed by the
782 butyryl-CoA dehydrogenase/Etf complex from Clostridium kluyveri. Journal of
783 Bacteriology **190:**843-850.
784 33. **Aboulnaga EH, Pinkenburg O, Schiffels J, El-Refai A, Buckel W, Selmer T.** 2013.
785 Effect of an Oxygen-Tolerant Bifurcating Butyryl Coenzyme A
786 Dehydrogenase/Electron-Transferring Flavoprotein Complex from Clostridium
787 difficile on Butyrate Production in Escherichia coli. Journal of Bacteriology
788 **195:**3704-3713.
789 34. **de Kok S, Meijer J, van Loosdrecht MC, Kleerebezem R.** 2013. Impact of dissolved
790 hydrogen partial pressure on mixed culture fermentations. Appl Microbiol
791 Biotechnol **97:**2617-2625.
792 35. **Buckel W, Thauer RK.** 2013. Energy conservation via electron bifurcating
793 ferredoxin reduction and proton/Na+ translocating ferredoxin oxidation.
794 Biochimica Et Biophysica Acta-Bioenergetics **1827:**94-113.
795 36. **Stams AJ, Plugge CM.** 2009. Electron transfer in syntrophic communities of
796 anaerobic bacteria and archaea. Nat Rev Microbiol **7:**568-577.
797 37. **Zhang F, Zhang Y, Chen M, van Loosdrecht MCM, Zeng RJ.** 2013. A modified
798 metabolic model for mixed culture fermentation with energy conserving electron
799 bifurcation reaction and metabolite transport energy. Biotechnol Bioeng **110:**1884-
800 1894.

801 38. **Rodriguez J, Kleerebezem R, Lema JM, van Loosdrecht MCM.** 2006. Modeling
802 product formation in anaerobic mixed culture fermentations. Biotechnol Bioeng
803 **93:**592-606.
804 39. **Balan V, Bals B, Chundawat SPS, Marshall D, Dale BE.** 2009. Lignocellulosic
805 Biomass Pretreatment Using AFEX. Biofuels: Methods and Protocols **581:**61-77.
806 40. **Parreiras LS, Breuer RJ, Avanasi Narasimhan R, Higbee AJ, La Reau A,**
807 **Tremaine M, Qin L, Willis LB, Bice BD, Bonfert BL, Pinhancos RC, Balloon AJ,**
808 **Uppugundla N, Liu T, Li C, Tanjore D, Ong IM, Li H, Pohlmann EL, Serate J,**
809 **Withers ST, Simmons BA, Hodge DB, Westphall MS, Coon JJ, Dale BE, Balan V,**
810 **Keating DH, Zhang Y, Landick R, Gasch AP, Sato TK.** 2014. Engineering and two-
811 stage evolution of a lignocellulosic hydrolysate-tolerant Saccharomyces cerevisiae
812 strain for anaerobic fermentation of xylose from AFEX pretreated corn stover. PLoS
813 One **9:**e107499.
814 41. **American Public Health Association WEF, and American Water Works**
815 **Association** 2005. Standard Methods for the Examination of Water and
816 Wastewater: 21st Edition. American Public Health Association.
817 42. **Yemm EW, Willis AJ.** 1954. The estimation of carbohydrates in plant extracts by
818 anthrone. Biochem J **57:**508-514.
819 43. **Joshi NA, Fass JN.** 2011. Sickle: A sliding-window, adaptive, quality-based trimming
820 tool for FastQ files (Version 1.33)
821 44. **Nurk S, Meleshko D, Korobeynikov A, Pevzner PA.** 2017. metaSPAdes: a new
822 versatile metagenomic assembler. Genome Res **27:**824-834.
823 45. **Wu YW, Simmons BA, Singer SW.** 2016. MaxBin 2.0: an automated binning
824 algorithm to recover genomes from multiple metagenomic datasets. Bioinformatics
825 **32:**605-607.
826 46. **Parks DH, Imelfort M, Skennerton CT, Hugenholtz P, Tyson GW.** 2015. CheckM:
827 assessing the quality of microbial genomes recovered from isolates, single cells, and
828 metagenomes. Genome Res **25:**1043-1055.
829 47. **Darling AE, Jospin G, Lowe E, Matsen FAt, Bik HM, Eisen JA.** 2014. PhyloSift:
830 phylogenetic analysis of genomes and metagenomes. PeerJ **2:**e243.
831 48. **Stamatakis A.** 2014. RAxML version 8: a tool for phylogenetic analysis and post-
832 analysis of large phylogenies. Bioinformatics **30:**1312-1313.
833 49. **Richter M, Rossello-Mora R, Oliver Glockner F, Peplies J.** 2016. JSpeciesWS: a
834 web server for prokaryotic species circumscription based on pairwise genome
835 comparison. Bioinformatics **32:**929-931.
836 50. **Hyatt D, Chen GL, Locascio PF, Land ML, Larimer FW, Hauser LJ.** 2010. Prodigal:
837 prokaryotic gene recognition and translation initiation site identification. BMC
838 Bioinformatics **11:**119.
839 51. **Kielbasa SM, Wan R, Sato K, Horton P, Frith MC.** 2011. Adaptive seeds tame
840 genomic sequence comparison. Genome Res **21:**487-493.
841 52. **Lawson CE, Wu S, Bhattacharjee AS, Hamilton JJ, McMahon KD, Goel R, Noguera**
842 **DR.** 2017. Metabolic network analysis reveals microbial community interactions in
843 anammox granules. Nat Commun **8:**15416.
844 53. **Kopylova E, Noe L, Touzet H.** 2012. SortMeRNA: fast and accurate filtering of
845 ribosomal RNAs in metatranscriptomic data. Bioinformatics **28:**3211-3217.

846 54. **Anders S, Pyl PT, Huber W.** 2015. HTSeq--a Python framework to work with high-
847 throughput sequencing data. Bioinformatics **31:**166-169.
848

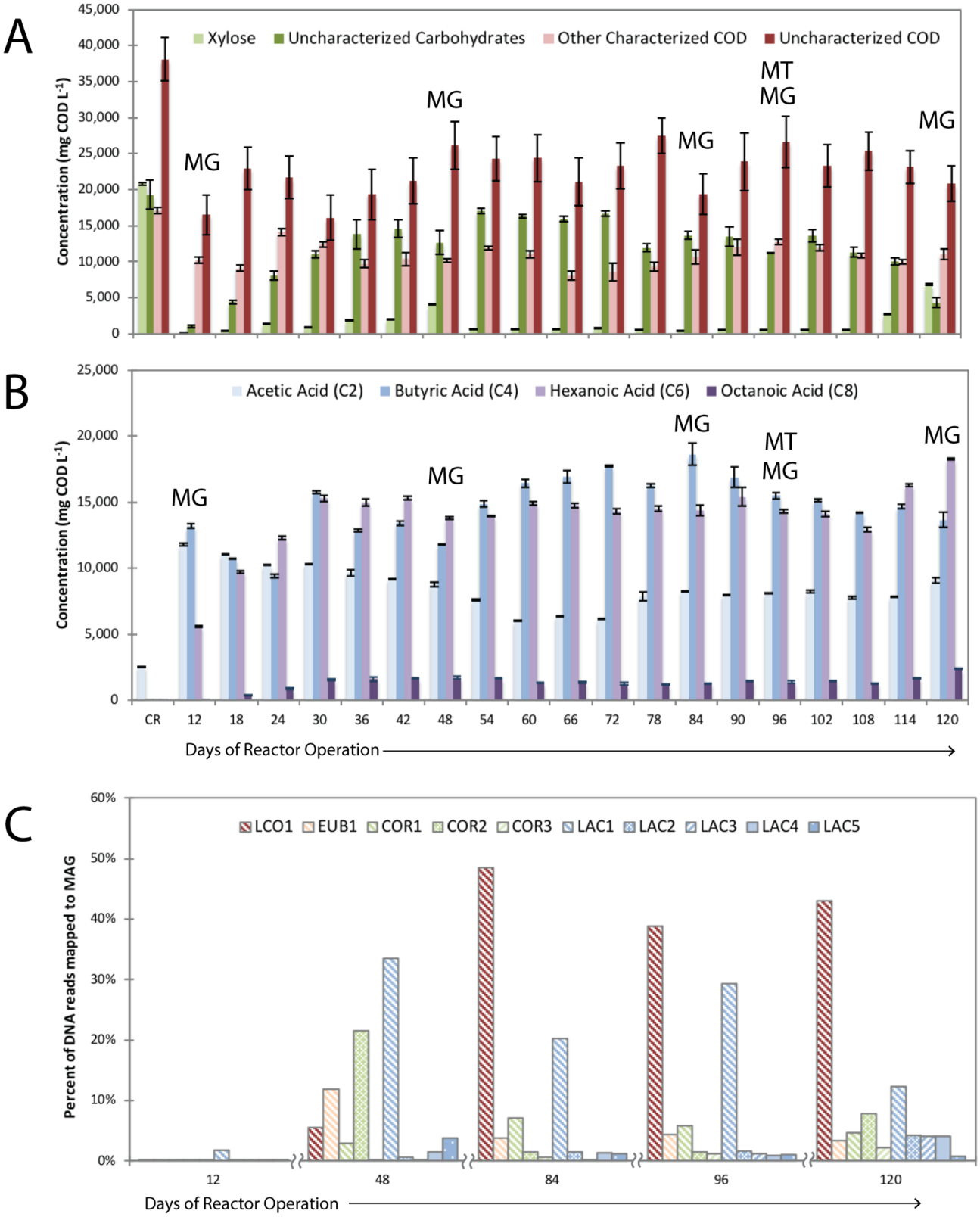
A
Xylose
Uncharacterized Carbohydrates
Other Characterized COD
Uncharacterized COD
Concentration (mg COD L-1)
MG
MG
MG
MT
MG
MG
B
Acetic Acid (C2)
Butyric Acid (C4)
Hexanoic Acid (C6)
Octanoic Acid (C8)
Concentration (mg COD L-1)
MG
MG
MG
MT
MG
MG
CR
Days of Reactor Operation
C
LCO1
EUB1
COR1
COR2
COR3
LAC1
LAC2
LAC3
LAC4
LAC5
Percent of DNA reads mapped to MAG
Days of Reactor Operation

849

850 **Fig. 1. Transformation of materials in lignocellulosic ethanol conversion residue by an anaerobic**
851 **microbiome and abundance of MAGs.** During 120 days of reactor operation, compounds in conversion
852 residue (CR) were converted to medium-chain fatty acids. **For (A) and (B),** the first set of bars in the figure
853 describe concentrations in the feed (CR), whereas the rest of the bars describe concentrations in the reactor. A
854 more detailed description of the operation of this reactor is presented elsewhere (4).Samples were taken for
855 metagenomic (MG) analysis from five timepoints (Day 12, Day 48, Day 84, Day 96, and Day 120 and for
856 metatranscriptomic analysis (MT) from one time point (Day 96). Overall, the bioreactor transformed xylose,
857 uncharacterized carbohydrates and uncharacterized COD to acetic (C2), butyric (C4), hexanoic (C6) and
858 octanoic (C8) acids. The microbial community was enriched in 10 MAGs.

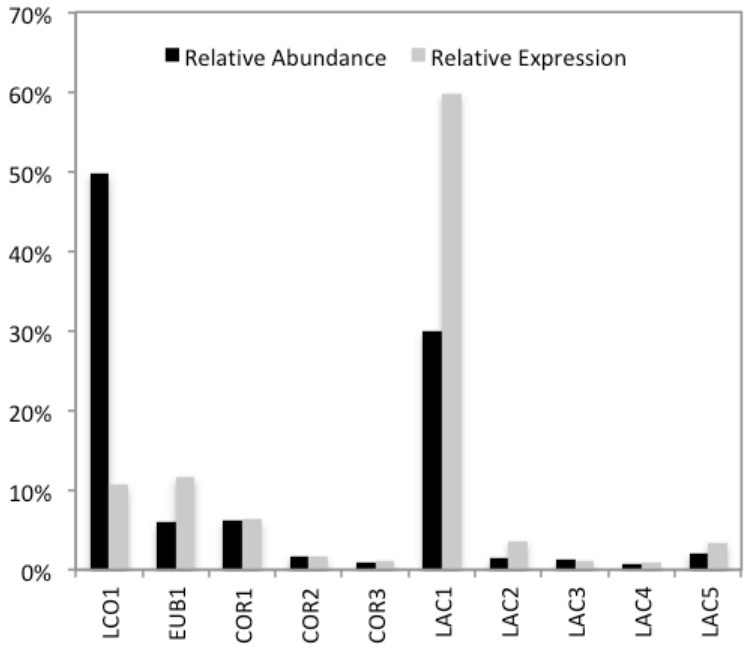

Fig. 2. Relative abundance and expression of the 10 most abundant MAGs in the bioreactor at Day 96. Relative abundance was determined by mapping DNA sequencing reads to the MAG and normalizing to the length of the MAG genome. Relative transcript abundance (expression) was determined by mapping c-DNA sequencing reads to the MAG and normalizing to the length of the MAG genome.

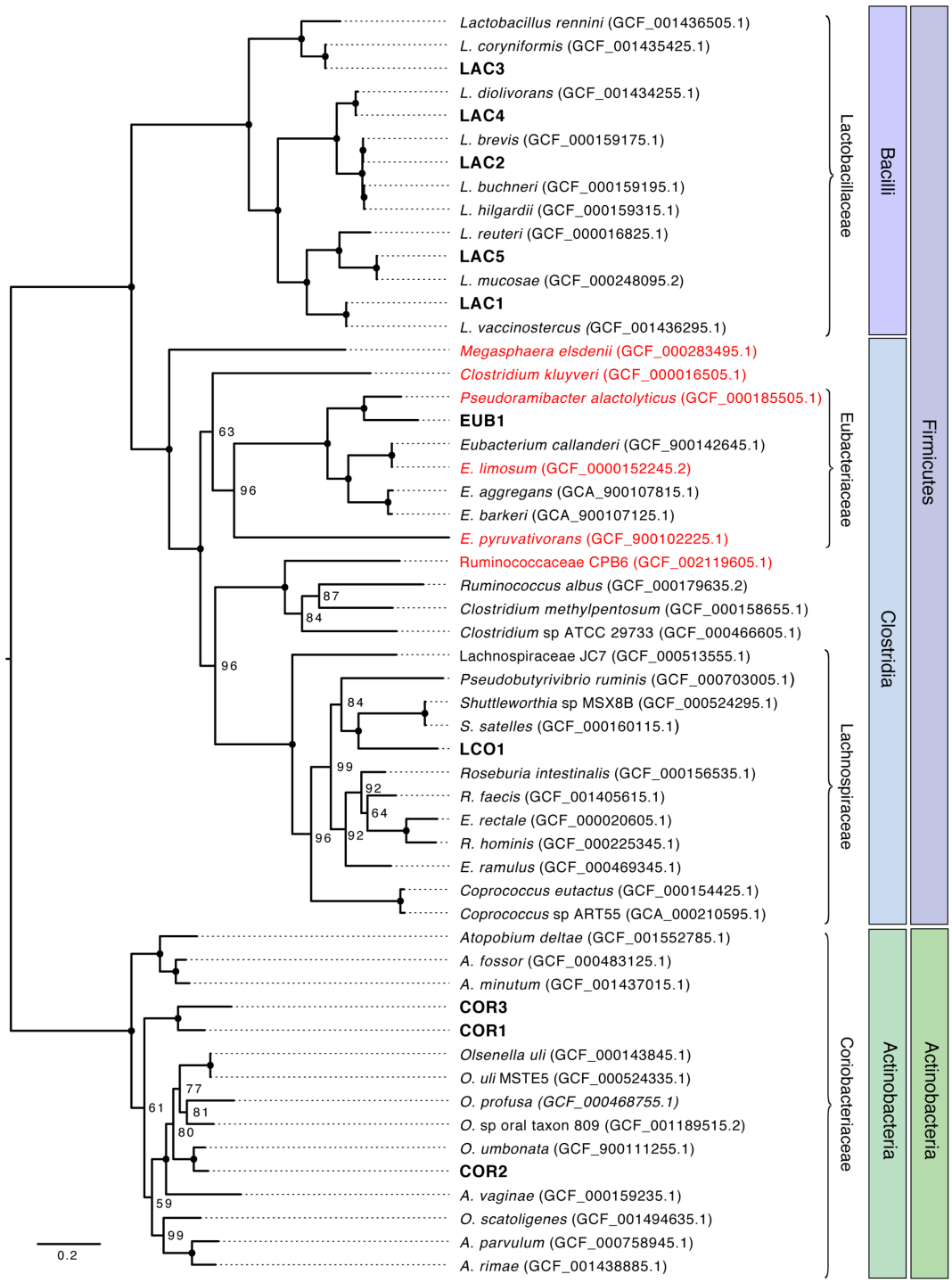

Fig. 3. Phylogenetic analysis for ten MAGs obtained from reactor biomass. Draft genomes from this study are shown in bold text. Red text indicates an organism that has been shown to produce MCFA. National Center for Biotechnology Information assembly accession numbers are shown in parentheses. Node labels represent bootstrap support values with solid circles representing a bootstrap support value of 100. The phyla and class of genomes are shown in shaded boxes and families are indicated by brackets For Actinobacteria genomes, Actinobacteria is both the phylum and class.

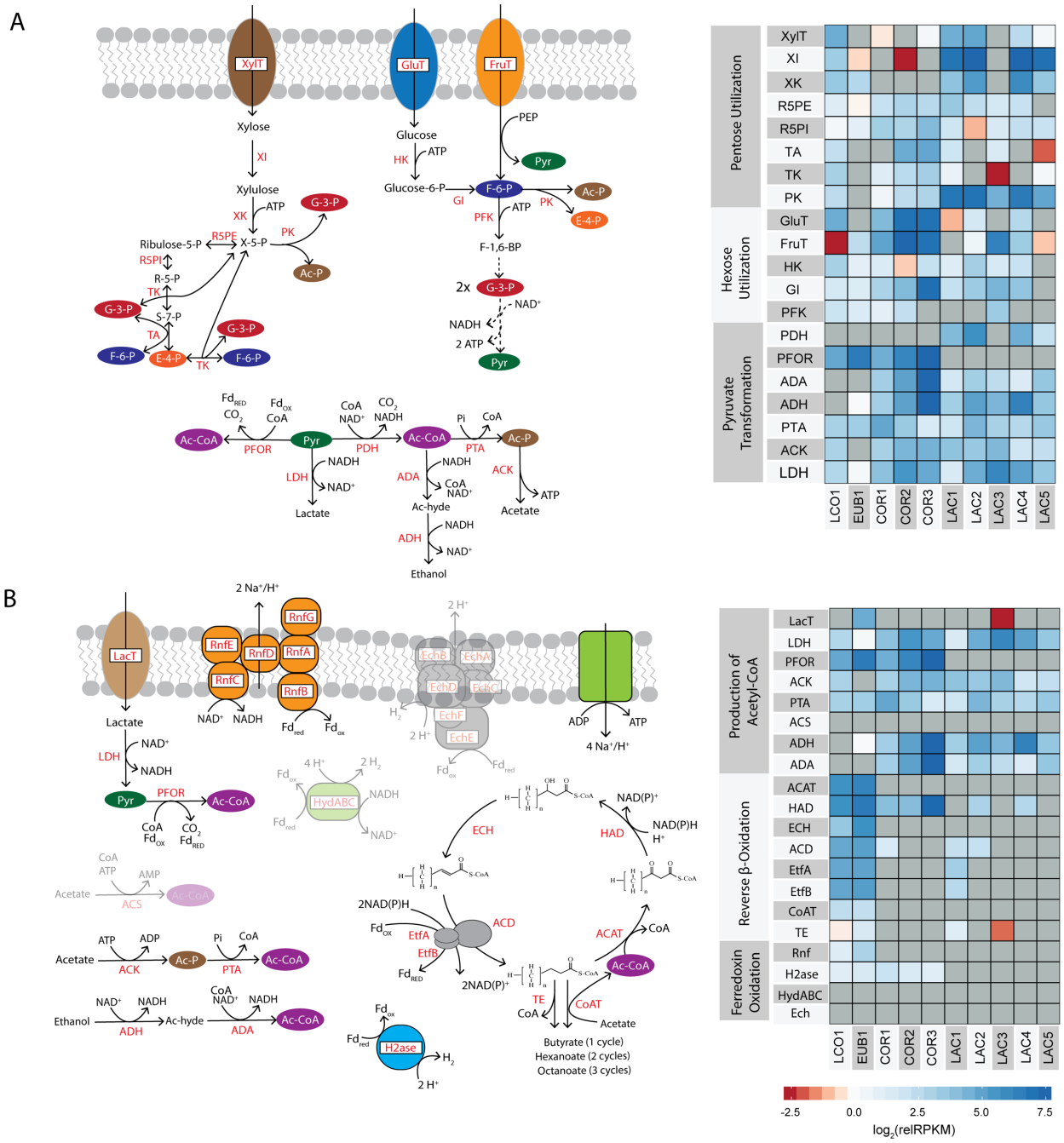

Fig. 4. Relative expression of genes involved in the conversion of xylose and lactate to MCFA. Expression of key enzymes involved in (**A**) the utilization of xylose, and **(B)** acyl chain elongation. Dashed lines represent the existence of multiple enzyme reactions between the indicated molecules. The relative RPKM (relRPKM) is normalized to the median RPKM for the MAG. Gene expression data is presented as the $\log_2$(relRPKM). The color intensities of the heatmaps represent the relative gene expression, with red color intensity indicating expression below median levels and blue intensity indicating expression above median levels. Grey indicates that the gene is absent from the genome. For genes that are not predicted to be expressed by any MAGs, the associated enzyme product is greyed out in the pathway figure. Key pathway intermediates include xylulose, xylulose-5-phosphate (X-5-P), ribose-5-phosphate (R-5-P), sedoheptulose-7-phosphate (S-7-P), erythyrose-4-phosphate (E-4-P), glyceraldehyde-3-phosphate (G-3-P), fructose-6-

886 phosphate (F-6-P), acetate (Ac), acetyl-phosphate (Ac-P), acetyl-CoA (Ac-CoA), lactate and ethanol. Enzyme
887 abbreviations are as follows: **(A)** XylT = xylose transporter, XI = xylose isomerase (EC 5.3.1.5); XK = xylulose
888 kinase (EC 2.7.1.17), R5PE = ribulose-5-phosphate epimerase (EC 5.1.3.1), R5PI = ribose-5-phosphate
889 isomerase (EC 5.3.1.6), TA = transaldolase (EC 2.2.1.2), TK = transketolase (EC 2.2.1.1), PK = D-xylulose 5-
890 phosphate/ D-fructose 6-phosphate phosphoketolase (EC 4.1.2.9), GluT = glucose transporter, FruT =
891 fructose PTS transporter, HK = hexokinase (EC 2.7.1.1, EC 2.7.1.2), G6PI =glucose-6-phoshphate isomerase
892 (EC 5.3.1.9), PFK = phosphofructokinase (EC 2.7.1.11), PDH = pyruvate dehydrogenase complex (EC 1.2.4.1,
893 EC 2.3.1.12, EC 1.8.1.4), PFOR = pyruvate flavodoxin oxidoreductase (EC 1.2.7.-), ADA = acetaldehyde
894 dehydrogenase (EC 1.2.1.10), AD = alcohol dehydrogenase (EC 1.1.1.1), PTA = phosphate acetyltransferase
895 (EC 2.3.1.8), ACK = acetate kinase (EC 2.7.2.1), LDH = lactate dehydrogenase (EC 1.1.1.27), **(B)** LacT = lactate
896 permease, ACS = acetyl-CoA synthetase (EC 6.2.1.1), ACAT = Acetyl-CoA C-acyltransferase (EC 2.3.1.16, EC
897 2.3.1.9), HAD = 3-Hydroxyacyl-CoA Dehydrogenase (EC 1.1.1.157, 1.1.1.35), ECH = Enoyl-CoA Hydratase (EC
898 4.2.1.55, EC 4.2.1.17), ACD = Acyl-CoA Dehydrogenase (EC 1.3.99.2, EC 1.3.99.-), EtfA = electron transfer
899 flavoprotein A, EtfB = electron transfer flavoprotein B, TE = thioesterase (EC 3.1.2.20), CoAT = 4-
900 Hydroxybutyrate CoA Transferase (EC 2.8.3.-), Rnf = ferredoxin: NAD^+ oxidoreductase - Na+ translocating (EC
901 1.18.1.8), H2ase = ferredoxin hydrogenase (EC 1.12.7.2), HydABC = bifurcating [Fe-Fe] hydorgenase (EC
902 1.12.1.4), Ech = energy conserving hydrogenase (EchABCDEF)
903

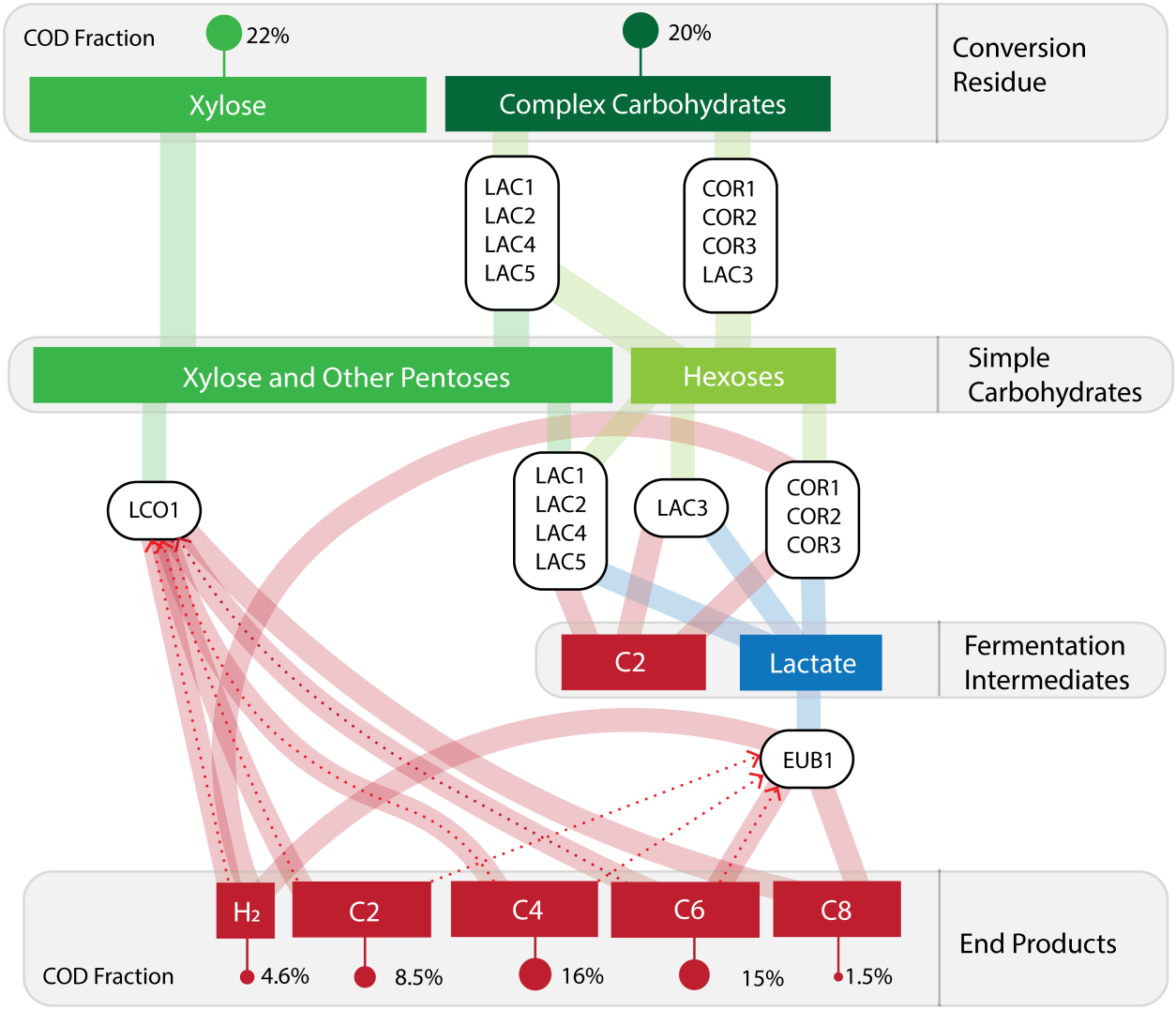

Fig. 5. Predicted transformations of major substrates in conversion residue to MCFA by this anaerobic microbiome. The microbes in the LAC and COR bins are predicted to produce sugars from complex carbohydrates. Simple carbohydrates, including xylose remaining in conversion residue, are converted to lactate and acetate by *Lactobacillus* (LAC) and Coriobacteriaceae (COR) MAGs. The Lachnospiraceae (LCO1) MAG converts pentoses directly to butyric acid (C4). The Eubacteriaceae (EUB1) produces hexanoic acid (C6) and octanoic acid (C8) from lactate. Further, LCO1 may utilize hydrogen to elongate C2 and C4 to MCFA, as represented by dashed lines. Additionally, EUB1 may elongate C2, C4 and C6 to C8.

913 **Table S1. Summary of MAGs obtained from DNA sequence analysis of the reactor microbiome.**
914 Taxonomy, completeness, and contamination were estimated with CheckM. Draft genomes were assembled
915 from five independent reactor samples. These MAGs represent the ten most abundant MAGs at Day 96 (Fig. 1).
916

Bin ID	Taxonomy	Completeness (%)	Contamination (%)	Genome size (bp)	# Scaffolds	N50	GC (%)	Predicted Genes
LCO1	Firmicutes; Clostridia; Clostridiales; Lachnospiraceae; Shuttleworthia	95.4	0.0	2,106,912	44	103,964	45.7	1,900
EUB1	Firmicutes; Clostridia; Clostridiales; Eubacteriaceae; Pseudoramibacter	97.8	0.2	2,002,609	35	142,846	51.2	1,857
COR1	Actinobacteria; Actinobacteria; Coriobacteriales; Coriobacteriaceae; Olsenella	99.2	0.8	2,512,349	225	22,880	59.0	2,358
COR2	Actinobacteria; Actinobacteria; Coriobacteriales; Coriobacteriaceae; Olsenella	100	1.6	2,422,853	155	34,678	64.8	2,185
COR3	Actinobacteria; Actinobacteria; Coriobacteriales; Coriobacteriaceae; Olsenella	98.4	7.4	3,647,413	533	13,368	55.5	4,068
LAC1	Firmicutes; Bacilli; Lactobacillales; Lactobacillaceae; Lactobacillus	99.5	1.1	2,633,889	18	640,122	43.6	2,567
LAC2	Firmicutes; Bacilli; Lactobacillales; Lactobacillaceae; Lactobacillus	99.4	1.6	3,179,174	79	122,889	40.5	2,989
LAC3	Firmicutes; Bacilli; Lactobacillales; Lactobacillaceae; Lactobacillus	99.2	1.4	2,704,063	174	29,509	43.0	2,731
LAC4	Firmicutes; Bacilli; Lactobacillales; Lactobacillaceae; Lactobacillus	98.9	1.3	3,335,227	95	86,779	40.2	3,150
LAC5	Firmicutes; Bacilli; Lactobacillales; Lactobacillaceae; Lactobacillus	80.1	0.8	1,487,044	181	12,363	46.1	1,524

917
918
919

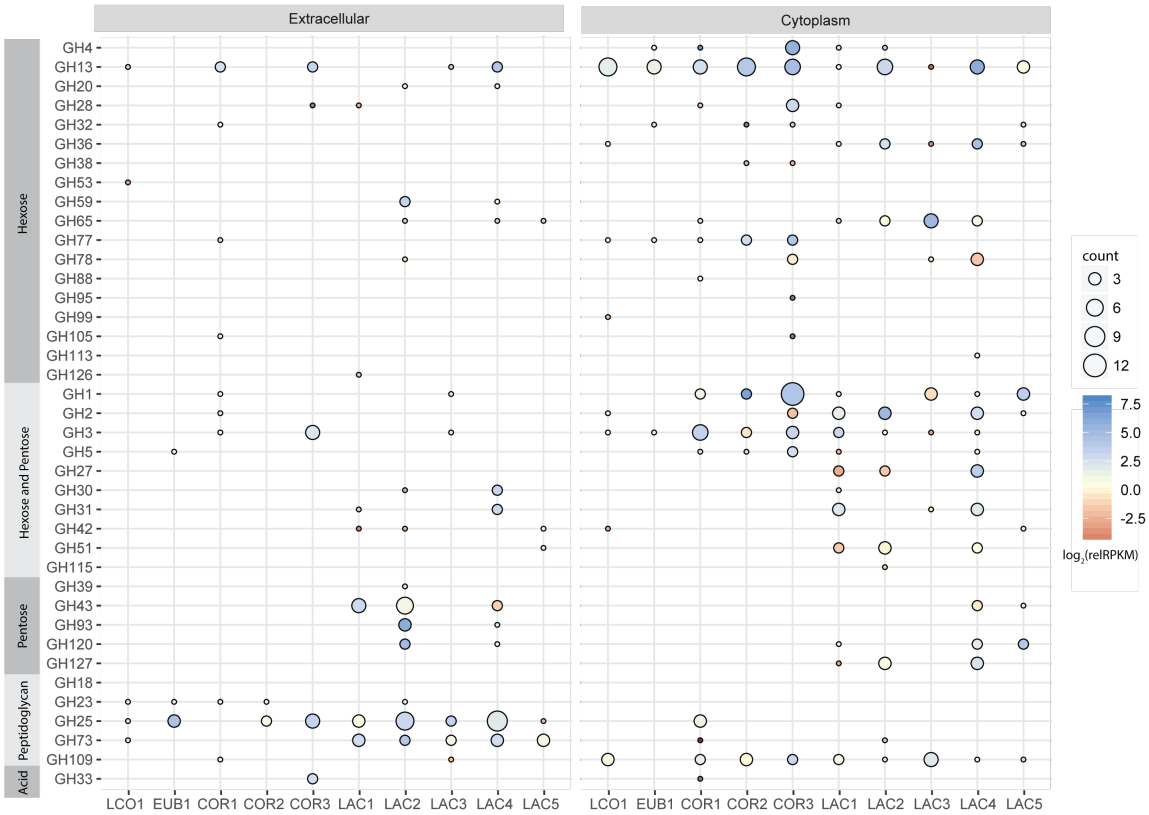

Fig. S1. Relative expression of extracellular and cytoplasmic glycoside hydrolase enzymes. Circle size indicates the number of ORFs annotated within each bin as the indicated CAZyme family. CAZyme families are grouped according to the target substrate moieties, being either bonds between hexoses only, bonds between both hexoses and pentoses, bonds between pentoses only, peptidoglycan-specific moieties, or acid moieties. The relative RPKM (relRPKM) is normalized to the median RPKM for the MAG. Gene expression data is presented as the $\log_2$(relRPKM). The color intensity represents the relative gene expression, with red color intensity indicating expression below median levels and blue intensity indicating expression above median levels. The represented expression is the highest relative expression for an individual gene within the indicated family. Descriptions of each family are available through the CAZY database (http://www.cazy.org/Glycoside-Hydrolases.html).

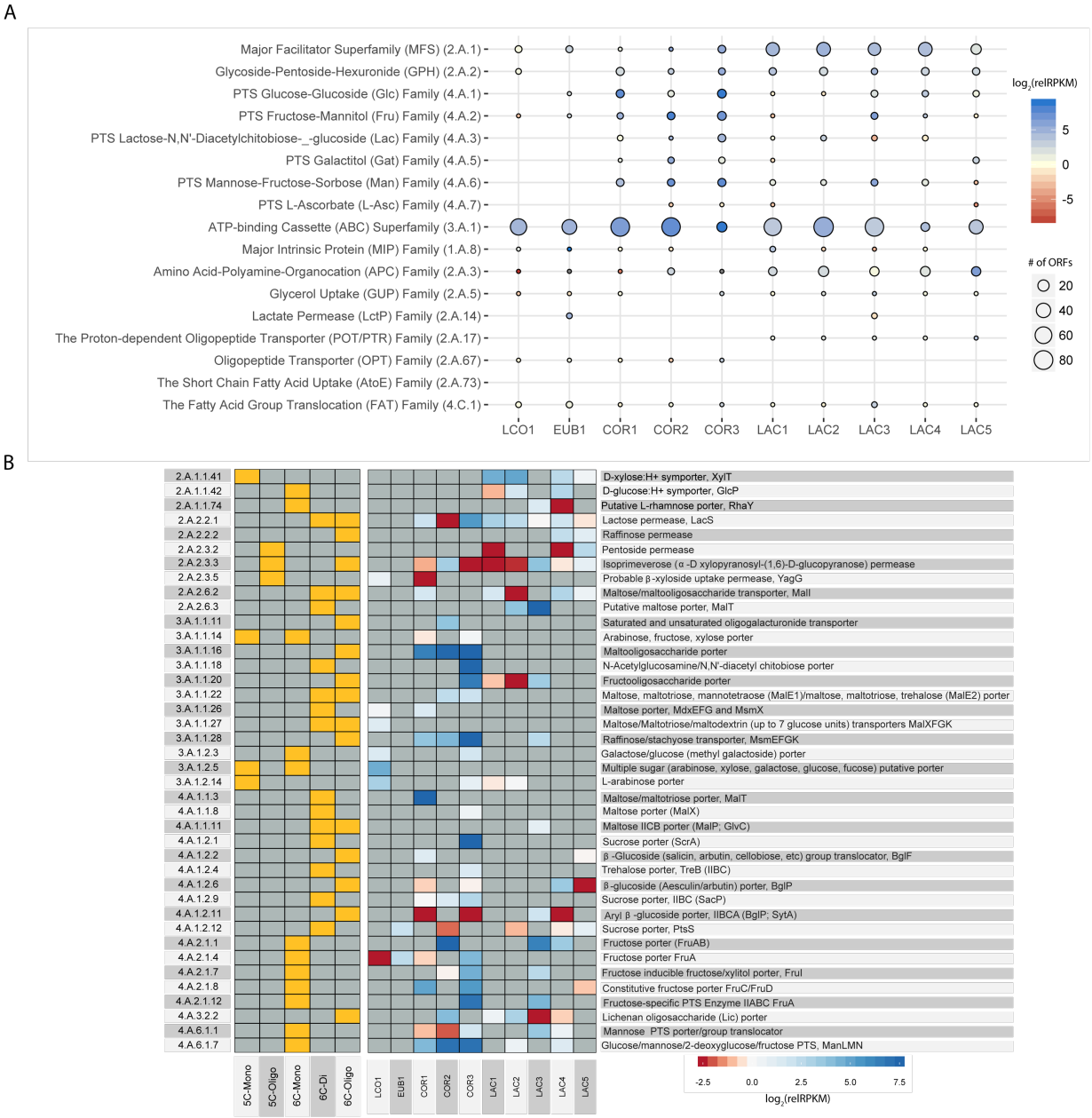

Fig. S2. Expression of known or predicted transporters by the 10 most abundant microbiome members. Transporters were annotated with the Transporter Classification Database. **(A)** The number of genes and relative expression for each analyzed MAG are shown for Transporter Database families. Circle size indicates the number of ORFs annotated within each bin as the indicated CAZY class or family. The color intensity represents the relative gene expression according to the shown scale. The represented expression is the highest relative expression for an individual gene within the indicated transporter family. (B) The expected substrates, either a pentose (5C-Mono), pentose-containing oligosaccharide (5C-Oligo), hexose (6C-mono), hexose disaccharide (6C-Di), or hexose-containing oligosaccharide (6C-Oligo) are indicated by orange squares. The color intensity represents the relative gene expression, with red color intensity indicating expression below median levels and blue intensity indicating expression above median levels. The transporter family ID and descriptions are shown. More detailed descriptions of transporters are available from the Transporter Database (http://www.tcdb.org).

Table S2. Thermodynamics of biochemical reactions involved in conversion of xylose to butyrate, hexanoate and octanoate. Free energies of formation for all chemical compounds were obtained from Kbase (www.kbase.us). The ATP yield was determined based on biochemical models presented in Supplement 7 and is indicated as mol ATP produced per mol xylose or lactate consumed. The terminal enzyme of reverse β-oxidation, either a CoA transferase (CoAT) or thioesterase (TE), is also indicated.

Eq No.	Equation	Associated MAG(s)	ΔG per mol substrate[1] (kJ mol^{-1})				$\Delta G^{0'}$available per ATP produced[2,3] (kJ mol^{-1} ATP)	Terminal Enzyme
			T = 35 °C P_{H2} =10-6 atm	T = 35 °C P_{H2} = 1 atm	T = 35 °C P_{H2} = 6.8 atm	Y_{ATP} (mol ATP mol^{-1} Substrate)[1,2]		
Xylose Simple Fermentation								
Eq. 1.	$3\ C_5H_{10}O_5 \rightarrow 5\ C_3H_5O_3^- + 5\ H^+$	LAC1, LAC2, LAC4, LAC5	-174	-174	-174	1.67	-104 to -104	-
Eq. 2.	$3\ C_5H_{10}O_5 \rightarrow 3\ C_3H_5O_3^- + 3\ C_2H_3O_2^- + 6\ H^+$	LAC1, LAC2, LAC4, LAC5	-214	-214	-214	2.00	-107 to -107	-
Xylose Elongation								
Eq. 3.	$3\ C_5H_{10}O_5 \rightarrow 3\ C_4H_7O_2^- + 3\ CO_2 + 3\ H_2O + 3\ H^+$	LCO1	-264	-264	-264	3.00	-88 to -88	CoAT
Eq. 4.	$3\ C_5H_{10}O_5 \rightarrow 1\ C_6H_{11}O_2^- + 3\ C_2H_3O_2^- + 3\ CO_2 + 4\ H^+ + 2\ H_2$	LCO1	-272	-248	-245	2.83	-87 to -96	CoAT
Eq. 5.	$3\ C_5H_{10}O_5 \rightarrow 1\ C_8H_{15}O_2^- + 2\ C_2H_3O_2^- + 3\ CO_2 + 3\ H_2O + 3\ H^+$	LCO1	-265	-265	-265	3.00	-88 to -88	CoAT
Eq. 6.	$2\ C_5H_{10}O_5 \rightarrow 1\ C_4H_7O_2^- + 2\ C_2H_3O_2^- + 2\ CO_2 + 3\ H^+ + 2\ H_2$	LCO1	-276	-240	-235	2.25	-105 to -123	TE
Eq. 7.	$3\ C_5H_{10}O_5 \rightarrow 1\ C_6H_{11}O_2^- + 3\ C_2H_3O_2^- + 3\ CO_2 + 1\ H_2O + 4\ H^+ + 2\ H_2$	LCO1	-272	-248	-245	2.50	-98 to -109	TE
Eq. 8	$4\ C_5H_{10}O_5 \rightarrow 1\ C_8H_{15}O_2^- + 4\ C_2H_3O_2^- + 4\ CO_2 + 2\ H_2O + 5\ H^+ + 2\ H_2$	LCO1	-270	-253	-250	2.63	-95 to -103	TE
Xylose and C2/ C4/ C6 Elongation								
Eq. 9	$1\ C_5H_{10}O_5 + 2\ C_2H_3O_2^- + 2\ H_2 \rightarrow 2\ C_4H_5O_2^- + 1\ CO_2 + 3\ H_2O$	LCO1	-240	-311	-320	3.50	-69 to -92	CoAT
Eq. 10	$1\ C_5H_{10}O_5 + 1\ C_2H_3O_2^- + 2\ H_2 \rightarrow 1\ C_6H_{11}O_2^- + 1\ CO_2 + 3\ H_2O$	LCO1	-240	-311	-320	3.50	-69 to -92	CoAT
Eq. 11	$1\ C_5H_{10}O_5 + 1\ C_4H_7O_2^- + 2\ H_2 \rightarrow 1\ C_8H_{15}O_2^- + 1\ CO_2 + 3\ H_2O$	LCO1	-264	-264	-264	3.50	-75 to -75	CoAT
Eq. 12	$1\ C_5H_{10}O_5 + 1\ C_4H_7O_2^- \rightarrow 1\ C_6H_{11}O_2^- + 1\ C_2H_3O_2^- + 1\ CO_2 + 1\ H_2O + 1\ H^+$	LCO1	-243	-314	-324	3.00	-81 to -108	CoAT
Eq. 13	$1\ C_5H_{10}O_5 + 1\ C_6H_{11}O_2^- \rightarrow 1\ C_8H_{15}O_2^- + 1\ C_2H_3O_2^- + 1\ CO_2 + 1\ H_2O + 1\ H^+$	LCO1	-267	-267	-267	3.00	-89 to -89	CoAT
Eq. 14	$1\ C_5H_{10}O_5 + 2\ C_2H_3O_2^- + 2\ H_2 \rightarrow 2\ C_4H_5O_2^- + 1\ CO_2 + 3\ H_2O$	LCO1	-240	-311	-320	1.50	-160 to -214	TE
Eq. 15	$1\ C_5H_{10}O_5 + 1\ C_2H_3O_2^- + 2\ H_2 \rightarrow 1\ C_6H_{11}O_2^- + 1\ CO_2 + 3\ H_2O$	LCO1	-240	-311	-320	2.50	-96 to -128	TE
Eq. 16	$1\ C_5H_{10}O_5 + 1\ C_4H_7O_2^- + 2\ H_2 \rightarrow 1\ C_8H_{15}O_2^- + 1\ CO_2 + 3\ H_2O$	LCO1	-264	-264	-264	2.50	-105 to -105	TE
Eq. 17	$1\ C_5H_{10}O_5 + 1\ C_4H_7O_2^- \rightarrow 1\ C_6H_{11}O_2^- + 1\ C_2H_3O_2^- + 1\ CO_2 + 1\ H_2O + 1\ H^+$	LCO1	-243	-314	-324	2.00	-122 to -162	TE
Eq. 18	$1\ C_5H_{10}O_5 + 1\ C_6H_{11}O_2^- \rightarrow 1\ C_8H_{15}O_2^- + 1\ C_2H_3O_2^- + 1\ CO_2 + 1\ H_2O + 1\ H^+$	LCO1	-267	-267	-267	2.00	-133 to -133	TE

1. ΔG values and expected ATP yields are normalized to mol of xylose, mol of lactate, or mol of glycerol
2. Pathway reconstructions shown in Supplement 7 were used to determine expected ATP yields.
3. The minimum expected DG0' released per mol ATP produced is 60 kJ. Values less than this are indicated by red text and indicate the predicted ATP yield exceeds what is phyiologically feasible

Table S3. Thermodynamics of biochemical reactions involved in conversion of lactate to butyrate, hexanoate and octanoate.

Eq No.	Equation	Associated MAG(s)	ΔG per mol substrate[1] (kJ mol^{-1})				$\Delta G^{0'}$ available per ATP produced[2,3] (kJ mol^{-1} ATP)	Terminal Enzyme
			T = 35 °C P_{H2} =10-6 atm	T = 35 °C P_{H2} = 1 atm	T = 35 °C P_{H2} = 6.8 atm	Y_{ATP} (mol ATP mol^{-1} Substrate)[1,2]		
Lactate Elongation								
Eq. 19	$2\ C_3H_5O_3^- + 1\ H^+ \rightarrow 1\ C_4H_7O_2^- + 2\ CO_2 + 2\ H_2$	EUB1	-62	-26	-21	0.75	-29 to -82	CoAT
Eq. 20	$3\ C_3H_5O_3^- + 2\ H^+ \rightarrow 1\ C_6H_{11}O_2^- + 3\ CO_2 + 2\ H_2 + 1\ H_2O$	EUB1	-58	-34	-31	0.83	-37 to -70	CoAT
Eq. 21	$4\ C_3H_5O_3^- + 3\ H^+ \rightarrow 1\ C_8H_{15}O_2^- + 4\ CO_2 + 2\ H_2 + 2\ H_2O$	EUB1	-57	-39	-36	0.88	-41 to -64	CoAT
Eq. 22	$2\ C_3H_5O_3^- + 1\ H^+ \rightarrow 1\ C_4H_7O_2^- + 2\ CO_2 + 2\ H_2$	EUB1	-62	-26	-21	0.25	-86 to -247	TE
Eq. 23	$3\ C_3H_5O_3^- + 2\ H^+ \rightarrow 1\ C_6H_{11}O_2^- + 3\ CO_2 + 2\ H_2 + 1\ H_2O$	EUB1	-58	-34	-31	0.50	-62 to -116	TE
Eq. 24	$4\ C_3H_5O_3^- + 3\ H^+ \rightarrow 1\ C_8H_{15}O_2^- + 4\ CO_2 + 2\ H_2 + 2\ H_2O$	EUB1	-57	-39	-36	0.63	-58 to -90	TE
Lactate and C2/ C4/ C6 Elongation								
Eq. 25	$1\ C_3H_5O_3^- + 1\ C_2H_3O_2^- + 1\ H^+ \rightarrow 1\ C_4H_7O_2^- + 1\ CO_2 + 1\ H_2O$	EUB1	-50	-50	-50	1.00	-50 to -50	CoAT
Eq. 26	$2\ C_3H_5O_3^- + 1\ C_2H_3O_2^- + 2\ H^+ \rightarrow 1\ C_6H_{11}O_2^- + 2\ CO_2 + 2\ H_2O$	EUB1	-50	-50	-50	1.00	-50 to -50	CoAT
Eq. 27	$3\ C_3H_5O_3^- + 1\ C_2H_3O_2^- + 3\ H^+ \rightarrow 1\ C_8H_{15}O_2^- + 3\ CO_2 + 3\ H_2O$	EUB1	-51	-51	-51	1.00	-51 to -51	CoAT
Eq. 28	$1\ C_3H_5O_3^- + 1\ C_4H_7O_2^- + 1\ H^+ \rightarrow 1\ C_6H_{11}O_2^- + 1\ CO_2 + 1\ H_2O$	EUB1	-50	-50	-50	1.00	-50 to -50	CoAT
Eq. 29	$2\ C_3H_5O_3^- + 1\ C_4H_7O_2^- + 2\ H^+ \rightarrow 1\ C_8H_{15}O_2^- + 2\ CO_2 + 2\ H_2O$	EUB1	-51	-51	-51	1.00	-51 to -51	CoAT
Eq. 30	$1\ C_3H_5O_3^- + 1\ C_6H_{11}O_2^- + 1\ H^+ \rightarrow 1\ C_8H_{15}O_2^- + 1\ CO_2 + 1\ H_2O$	EUB1	-53	-53	-53	1.00	-53 to -53	CoAT
Eq. 31	$1\ C_3H_5O_3^- + 1\ C_2H_3O_2^- + 1\ H^+ \rightarrow 1\ C_4H_7O_2^- + 1\ CO_2 + 1\ H_2O$	None[4]	-50	-50	-50	0.00	NA[5]	TE
Eq. 32	$2\ C_3H_5O_3^- + 1\ C_2H_3O_2^- + 2\ H^+ \rightarrow 1\ C_6H_{11}O_2^- + 2\ CO_2 + 2\ H_2O$	None[4]	-50	-50	-50	0.50	-100 to -100	TE
Eq. 33	$3\ C_3H_5O_3^- + 1\ C_2H_3O_2^- + 3\ H^+ \rightarrow 1\ C_8H_{15}O_2^- + 3\ CO_2 + 3\ H_2O$	None[4]	-51	-51	-51	0.67	-76 to -76	TE
Eq. 34	$1\ C_3H_5O_3^- + 1\ C_4H_7O_2^- + 1\ H^+ \rightarrow 1\ C_6H_{11}O_2^- + 1\ CO_2 + 1\ H_2O$	None[4]	-50	-50	-50	0.00	NA[5]	TE
Eq. 35	$2\ C_3H_5O_3^- + 1\ C_4H_7O_2^- + 2\ H^+ \rightarrow 1\ C_8H_{15}O_2^- + 2\ CO_2 + 2\ H_2O$	None[4]	-51	-51	-51	0.50	-103 to -103	TE
Eq. 36	$1\ C_3H_5O_3^- + 1\ C_6H_{11}O_2^- + 1\ H^+ \rightarrow 1\ C_8H_{15}O_2^- + 1\ CO_2 + 1\ H_2O$	None[4]	-53	-53	-53	0.00	NA[5]	TE

1. ΔG values and expected ATP yields are normalized to mol of xylose, mol of lactate, or mol of glycerol
2. Pathway reconstructions shown in Supplement 7 were used to determine expected ATP yields.
3. The minimum expected ΔG0' released per mol ATP produced is 60 kJ. Values less than this are indicated by red text and indicate the predicted ATP yield exceeds what is phyiologically feasible
4.The proposed model requires ACK for either incorporation of a carboxylate or for ATP generation from acetyl-CoA. EUB1 is not predicted to produce this enzyme.
5. No net ATP production is predicted for this model.